Research Paper

THEMED ISSUE: Anatomy of Rifting: Tectonics and Magmatism in Continental Rifts, Oceanic Spreading Centers, and Transforms

GEOSPHERE

GEOSPHERE; v. 14, no. 2

doi:10.1130/GES01522.1

6 figures; 13 tables

CORRESPONDENCE: jolante.vanwijk@nmt.edu

CITATION: van Wijk, J., Koning, D., Axen, G., Coblentz, D., Gragg, E., and Sion, B., 2018, Tectonic subsidence, geoid analysis, and the Miocene-Pliocene unconformity in the Rio Grande rift, southwestern United States: Implications for mantle upwelling as a driving force for rift opening: Geosphere, v. 14, no. 2, p. 684–709, doi:10.1130/GES01522.1.

Science Editor: Raymond M. Russo
Guest Associate Editor: Tyrone O. Rooney

Received 1 March 2017
Revision received 30 November 2017
Accepted 30 January 2018
Published online 25 February 2018

Tectonic subsidence, geoid analysis, and the Miocene-Pliocene unconformity in the Rio Grande rift, southwestern United States: Implications for mantle upwelling as a driving force for rift opening

Jolante van Wijk[1], Daniel Koning[2], Gary Axen[1], David Coblentz[3], Evan Gragg[1], and Brad Sion[1]

[1]Department of Earth and Environmental Science, New Mexico Institute of Mining and Technology, 801 Leroy Place, Socorro, New Mexico 87801, USA
[2]New Mexico Bureau of Geology and Mineral Resources, New Mexico Institute of Mining and Technology, 801 Leroy Place, Socorro, New Mexico 87801, USA
[3]Los Alamos National Laboratory, Los Alamos, New Mexico 87545, USA

ABSTRACT

We use tectonic subsidence patterns from wells and stratigraphic sections to describe the mid-Miocene to present tectonic subsidence history of the Rio Grande rift. Tectonic subsidence and therefore rift opening were quite fast until ca. 8 Ma, with net subsidence rates (~25–65 mm/k.y.) comparable to those of the prerupture phase of rifted continental margins. The rapid subsidence was followed by a late Miocene–early Pliocene unconformity that developed mainly along the flanks of most rift basins. The age of its associated lacuna is spatially variable but falls within 8–3 Ma (mostly 7–5 Ma) and thus is synchronous with eastward tilting of the western Great Plains (ca. 6–4 Ma). Tectonic subsidence rates either remained similar or decreased after the Miocene-Pliocene unconformity. North of 35°N, our analysis of geoid-to-elevation ratios suggests that, at present, topography of the Rio Grande rift region is compensated by a component of mantle-driven dynamic uplift. Previous work has indicated that this dynamic uplift is caused by focused vertical flow in the upper mantle resulting from slab descent and fragmentation of the Farallon slab, and Rio Grande rift opening, which affected the Rio Grande rift area beginning in the late Miocene. The spatial distribution and timing of the unconformity, as well as eastward tilting of the western Great Plains, can be explained by this dynamic mantle uplift, with contributions from variations in rift opening tectonics and climate. The focused mantle upwelling is not associated with increased rift opening rates.

INTRODUCTION

Since the pioneering work of early geologists (Bryan, 1938; Kelley, 1952; Chapin, 1971), the Rio Grande rift in Colorado, New Mexico, and western Texas (Figs. 1 and 2) has been considered one of the classic continental rifts on Earth. The rift is defined by a series of mainly north-trending, half-graben sedimentary basins that extend from the upper Arkansas basin of central Colorado to west Texas and adjacent Mexico (Fig. 1; e.g., Chapin and Cather, 1994). The northern Rio Grande rift is only one basin wide, but structural complexities

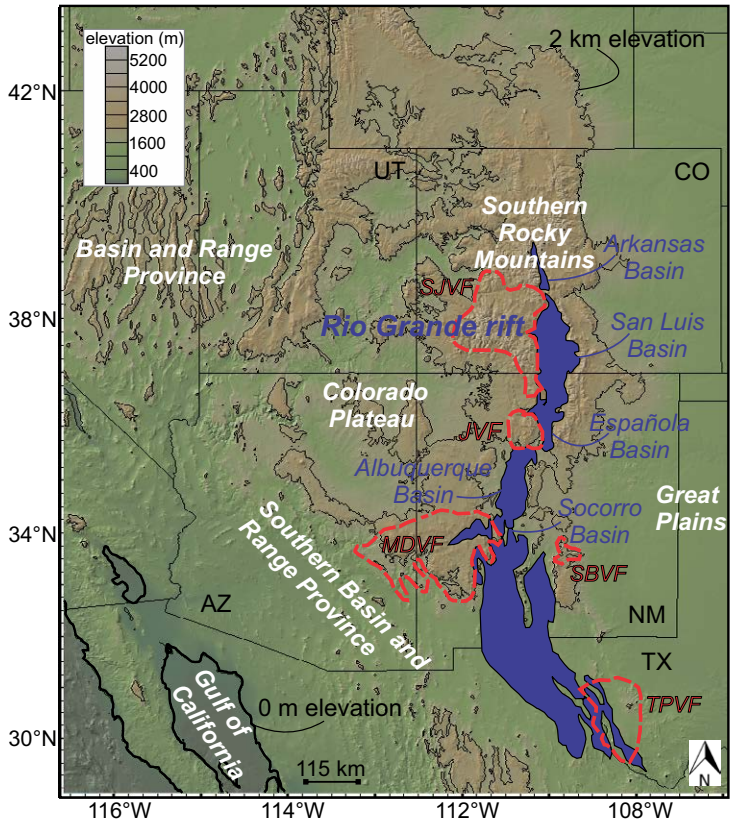

Figure 1. Topographic map with tectonic setting of the Rio Grande rift (blue) in the western United States, and Paleogene volcanic fields (red dashed lines). JVF—Jemez volcanic field, MDVF—Mogollon-Datil volcanic field, SBVF—Sierra Blanca volcanic field, SJVF—San Juan volcanic field, TPVF—Trans-Pecos volcanic field. State abbreviations: UT—Utah, CO—Colorado, AZ—Arizona, NM—New Mexico, TX—Texas.

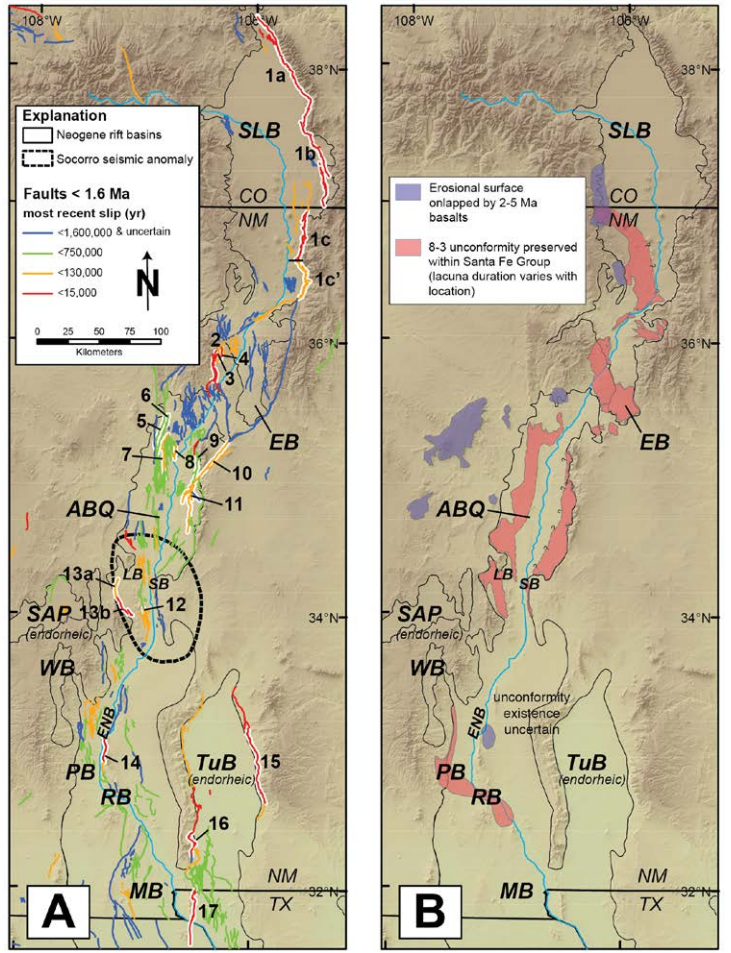

Figure 2. Map of major Neogene basins of the Rio Grande rift showing (A) middle-late Quaternary faults and (B) mappable areas of the Miocene-Pliocene unconformity. Delineation of the Socorro seismic anomaly is shown in A. Faults active since 1.6 Ma are categorized according to most recent surface-rupture event. ABQ—Albuquerque Basin, EB—Española Basin, ENB—Engle Basin, LB—La Jencia Basin, MB—Mesilla Basin, PB—Palomas Basin, RB—Rincon Basin, SAP—San Agustin Plains, SB—Socorro Basin, SLB—San Luis Basin, TuB—Tularosa Basin, WB—Winston Basin. State abbreviations: CO—Colorado, NM—New Mexico, TX—Texas. Numerals are keyed to specific faults in Table 1. Highlighted faults have been trenched.

result in subbasins within its larger basins (e.g., Albuquerque Basin—Grauch and Connell, 2013; Española Basin—Ferguson et al., 1995; Koning et al., 2013; San Luis Basin—Brister and Gries, 1994). The northern Rio Grande rift is thus a typical narrow rift zone. South of the Albuquerque Basin, the rift widens east-west so that up to four basins are present at a given latitude, separated by uplifted ranges (e.g., northern Tularosa, Engle, Palomas, and Winston Basins; Fig. 2). The southern Rio Grande rift, south of the Albuquerque Basin (Fig. 1), gradually merges with the southern Basin and Range Province and is best described as a wide continental rift. Many of the basins are bounded by faults with Quaternary scarps (Figs. 2 and 3; Table 1; e.g., Machette, 1986), attesting to continued tectonic activity in the rift.

The development and the structural and stratigraphic characteristics of continental rifts are the result of many processes and their interactions, such as rheology of the lithosphere, magmatism, upper-mantle buoyancy, (inherited) structures, climate, and surface processes (Burov and Poliakov, 2001; Lavier and Buck, 2002; Corti et al., 2003; van Wijk, 2005; Bialas et al., 2010; Esedo et al., 2012; Brune et al., 2014; Ricketts et al., 2015; Ricketts and Karlstrom, 2016; Repasch et al., 2017; and many others). The roles these processes play in Rio Grande rift formation are not fully understood. Recent studies have pointed to an important component of mantle dynamics in both the earlier and later rift phases (van Wijk et al., 2008; Moucha et al., 2008; Esedo et al., 2012; Karlstrom et al., 2012; Nereson et al., 2013; Ricketts et al., 2015; Ricketts and Karlstrom, 2016; Repasch et al., 2017), expressed in elevation, erosional patterns, and river incision profiles. Here, we focus on a lacuna in the Rio Grande rift that may be related to mantle buoyancy. The unconformity has previously been described in several localities (e.g., Bryan, 1938; Stearns, 1953, 1979; Cather et al., 1994; Chapin and Cather, 1994; Connell et al., 2013; Nereson et al., 2013; Koning et al., 2016a) and explained in terms of climate change (Chapin, 2008) or slowing down of tectonic rift opening (Cather et al., 1994). Field studies (e.g., Bryan, 1938; Stearns, 1953, 1979; Cather et al., 1994; Connell et al., 2013) have described the lacuna in places (Fig. 2) as an (angular) unconformity, where pre-unconformity strata (mid- to late Miocene) generally have steeper dips than postunconformity Pliocene–Pleistocene basin fill. The younger, less-deformed strata include deposits related to fluvial integration of rift basins in the Rio Grande rift during formation of the Rio Grande River (Mack et al., 1998, 2006; Connell et al., 2005; Nereson et al., 2013; Repasch et al., 2017). In this study, we mapped all locations where the unconformity has been described to understand its spatial distribution in the rift. When combined with analysis of tectonic subsidence curves of 11 stratigraphic columns in the rift zone, we found that the Miocene-Pliocene unconformity is widespread, and it is also inferred to occur outside the rift zone (in the Raton-Clayton and Ocate volcanic field [Nereson et al., 2013], and possibly in the Rio San Jose, west of the Albuquerque Basin [Channer et al., 2015]). We interpret that it may be synchronous with eastward tilting of the Ogallala Formation, east of the Rio Grande rift on the western Great Plains. The cause of this unconformity is currently debated (Cather et al., 1994; Chapin, 2008; Connell et al., 2013; Nereson et al., 2013), and because earlier studies did not appreciate its spatial extent, an evaluation of postulated explanations is needed. We used geoid-topography analysis to ascertain the nature of present-day topographic compensation of the Rio Grande rift region.

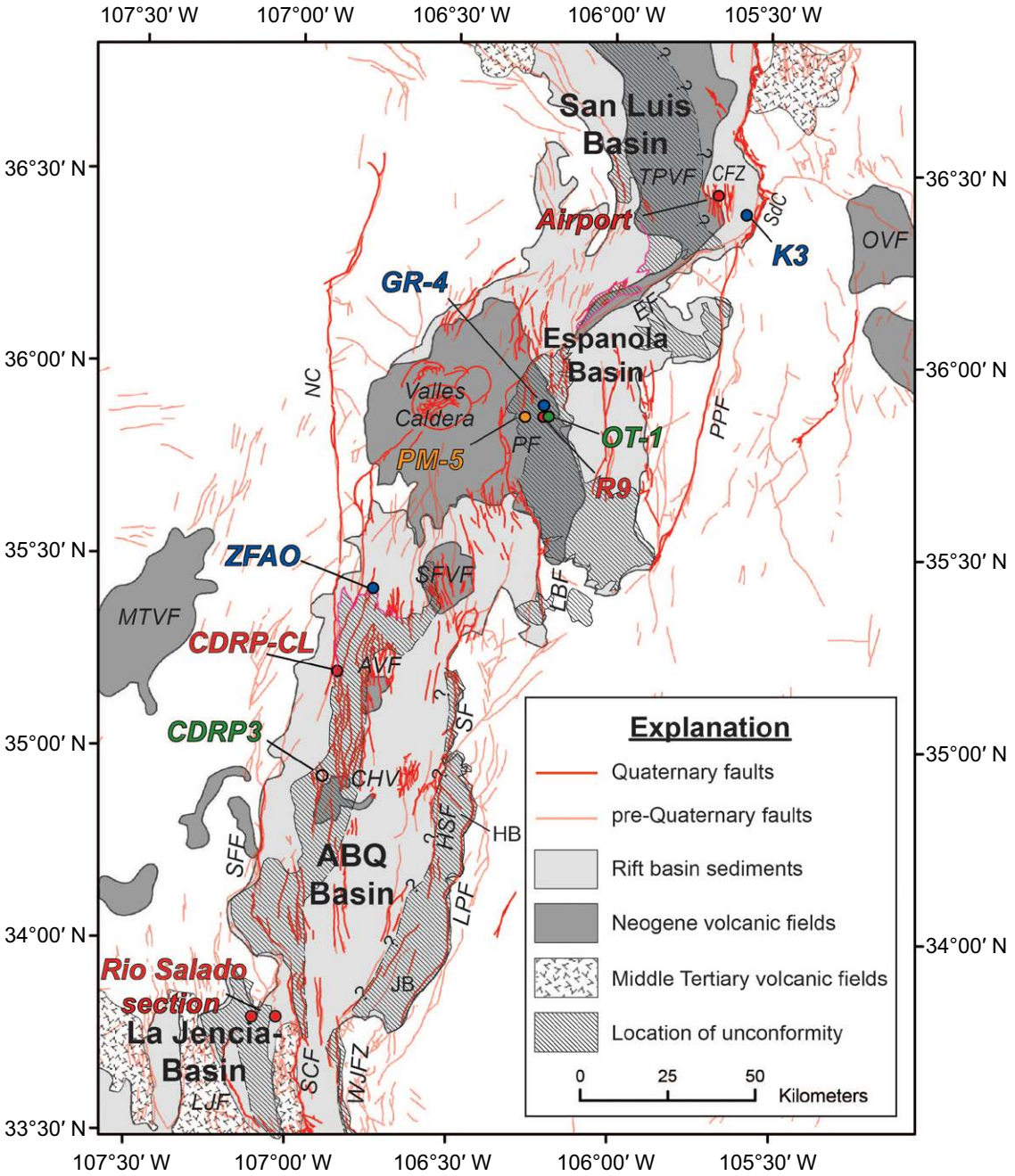

Figure 3. Map of north-central Rio Grande rift with locations of wells and stratigraphic section used for tectonic subsidence models. Quaternary faults are in red. Colored, large text indicates locations (wells and stratigraphic sections) for which stratigraphic data were used in models (Tables 3–13). ABQ—Albuquerque. Volcanic fields: AVF—Albuquerque, CHV—Cat Hills, MTVF—Mount Taylor, OVF—Ocate, SFVF—San Felipe, TPVF—Taos Plateau. Faults (F) and fault zones (FZ): EF—Embudo, HSF—Hubble Springs, LBF—La Bajada, LJF—La Jencia, LPF—Los Pinos–Manzano, NC—Nacimiento, PF—Pajarito fault, PPF—Pecos-Picuris, SCF—Socorro Canyon, SF—Sandia-Rincon, SFF—Santa Fe–Coyote–Moquino, WJFZ—west Joyita. Miocene-Pliocene unconformity is shown by the hatch pattern. Well-exposed margins of the unconformity with age control are shown by the pink-purple line for the southwestern San Luis Basin (Koning et al., 2016a; Repasch et al., 2017) and Albuquerque Basin (Connell et al., 1999, 2013). Following Connell et al. (2013), we infer that the unconformity is present on the Joyita and Hubbell structural benches (labeled JB and HB, respectively) in the southeastern Albuquerque Basin. CFZ—Los Cordovas faults; SdC—Sangre de Cristo fault.

TABLE 1. QUATERNARY FAULTS IN THE RIO GRANDE RIFT (LOCATIONS SHOWN IN FIG. 2)

Fault (no. in Fig. 2)	Age of most recent surface rupture(s)*	Recurrence interval/*slip rate*	Average vertical displacement per event	Reference
Northern Sangre de Cristo (1a)	5–8 [8–13, 13–35] ka	3–40 ka 0.1–0.2 mm/yr	1.5–2.5 m	McCalpin (1982, 1986, 2006), Ruleman and Machette (2007)
Central Sangre de Cristo (1b)	9 ± 2 ka	Ca. 12 ka *0.17 mm/yr during late Pleistocene*	2.3 m	Crone and Machette (2005)
Southern Sangre de Cristo, Latir Peaks section (1c)†	Holocene	*0.18 mm/yr over past 3.9 m.y.;* *0.04 mm/yr since late middle Pleistocene*		Ruleman et al. (2013)
Southern Sangre de Cristo, south part (1c′)†	10–30 ka	Tens of thousands of years		Kelson et al. (2004)
Pajarito (2)	1.4§ ka, 6.5–5.2 ka, early Holocene	20–40 ka *0.1 mm/yr#*		McCalpin (2005), Reneau et al. (2002)
Rendija Canyon (3)**	9 or 23 ka	33–83 ka *0.03 ± 0.1 mm/yr*	2.0 ± 0.5 m	Wong et al. (1995), Kelson et al. (1996)
Guaje Mountain (4)**	6.5–4.0 ka [ca. 39, 144–300 ka]	Tens of thousands of years; *0.01 mm/yr since 1.2 Ma*	0.5–2.0 m	Gardner et al. (2003), Wong et al. (1995)
Calabacillas (5)	14 ka	10–20 ka *0.011–0.028 mm/yr*	0.3 m	McCalpin et al. (2011)
Zia (6)†	11 ka	10–21 ka *0.055–0.1 mm/yr*	1.3 m	McCalpin and Harrison (2001)
County Dump (7)	28 or 47–34 ka	Tens of thousands of years *0.02–0.05 mm/yr*	1.4 ± 0.7 m	McCalpin (1997), Personius et al. (1999)
East Paradise fault zone (8)	10–80 ka	80–150 ka	0.5–1.3 m	Personius et al. (1999)
Sandia (9)	53–67 ka††		1.6	McCalpin and Harrison (2006)
Tijeras (10)†	10–130 ka			Kelson et al. (1999)
Hubbell Spring (11)	15–6 ka	14–27 ka *0.2–1.0 mm/yr*	0.4–3.7 m (vertical)	Olig et al. (2011), Personius and Mahan (2003)
Socorro Canyon (12)	Late Holocene	Ca. 30–70 ka *0.04 mm/yr*	1.5–2.0 m	Phillips et al. (2003)
La Jencia, north part (13a)	3, 28–40, 150 ka§§	Ca. 100 ka	1.5–4.5 m	Machette (1986)
La Jencia, south part (13b)	5–6, 15 ka		1–5 m	Machette (1986)
Caballo (14)	1.6–5.0 ka	50–100 ka *0.02–0.03 mm/yr*	1.25–2.6 m	Foley et al. (1988), Machette et al. (1998)
Alamogordo, south part (15)	8–10; 10.5–11.2 ka##	Tens of thousands of years***	1–6 m	Koning and Pazzaglia (2002), Koning (1999)
Organ Mountains (16)	1–5 ka	4–15 ka, poorly constrained	As much as 5 m	Gile (1986, 1994), Machette (1987)
East Franklin Mountains (17)	13–17 ka	14–19 ka *0.18 mm/yr for late Pleistocene;* *0.145 mm/yr post–500 ka*	~3-4.5 m	McCalpin (2006)

Note: Only faults with paleoseismic data from detailed trench or exposure studies are included.
*Brackets denote penultimate and third-most-recent events.
†Age control based solely on soil development.
§The 1.4 ka event is only interpreted from one trench (out of 14); there is more evidence for a 6.5–5.2 ka most recent event.
#Slip rate slowed after ca. 1 Ma.
**These faults belong to the Pajarito fault system.
††Only one strand out of four were trenched; paleoseismic parameters must be viewed as very incomplete.
§§The penultimate event is estimated to be 150 ± 50 ka for all parts of the section. Evidence of Holocene movement is only on one subsection, and Machette et al. (1998) interpreted the last rupture event for the entire section as occurring <150 ka.
##Fault appears to be segmented, with unique last-rupture events on the two segments.
***Two large-displacement events interpreted to occur within 2000–4000 yr ca. 13 ka.

The geoid-topography ratio provides a means with which to understand the role of the upper mantle as an uplift mechanism. Our results suggest that a regional mantle-driven uplift event promoted development of the unconformity and concomitant Ogallala Formation tilting. This is noteworthy, since the Rio Grande rift lacks the typical characteristics of mantle-driven rifts ("active rifting"), such as large-volume volcanism caused by a mantle plume (Turcotte and Emerman, 1983). Implications of this major epeirogenic uplift event that has affected the Rio Grande rift in the last 8 m.y. or so are discussed in relation to upper-mantle driving forces for rifting.

BACKGROUND

The stratigraphic data sets that we used for the tectonic subsidence analyses provide information for the rift-opening period between ca. 15 and 2 Ma. Extension in the rift started, however, much earlier, and rift opening has continued throughout the Quaternary to the present day. Aspects of these early and late phases of opening are summarized next. These sections are followed by a description of the Miocene-Pliocene unconformity.

Onset and Cause of Rio Grande Rift Opening

Extension of the southern Rio Grande rift began as early as 38–35 Ma, coeval with volcanism in the Mogollon-Datil and Sierra Blanca volcanic fields (Fig. 1). In the northeastern Mogollon-Datil area, sedimentary thickness patterns across faults indicate that preexisting Laramide faults were reactivated as normal faults after 36 Ma (Cather, 1990), and southeast of the volcanic field, an east-tilted half graben developed by 36–35 Ma (Mack et al., 1994a, 1994b). Northeast-trending dike swarms in the Sierra Blanca volcanic field and geologic map relations (upward fault terminations and stratal tilts) have been used to interpret northwest-southeast extension between 38 and 34.3 Ma (Koning et al., 2014). Approximately northwest-southeast extension became prevalent after ca. 32–30 Ma, contemporaneous with voluminous volcanism in the Trans-Pecos, Mogollon-Datil, and San Juan volcanic fields (e.g., Morgan et al., 1986). As such, the earliest Rio Grande rift opening can be considered intra- or back-arc extension. In west Texas, the stress field, as recorded by dikes and veins, changed ca. 32–30 Ma from approximately east-west Laramide contraction to approximately ENE-WSW–directed extension, but normal faulting did not begin until ca. 24–23 Ma (Henry and Price, 1986).

Extension initiated later in the northern rift (30–26 Ma, possibly 33–26 Ma) than the southern rift (38–34 Ma). Angular unconformities related to the onset of extension in the San Luis and Española Basins are bracketed at 28–27 Ma and 30–26 Ma, respectively (Lipman and Mehnert, 1975; Koning et al., 2013). In these basins, ca. 27–25 Ma basalt and tuff are intercalated with basal Santa Fe Group clastics. Tweto (1979) inferred an earlier onset of extension in the San Luis Basin from limited subsurface data, and Chapin and Cather (1994) speculated that plutons as old as 33 Ma around the upper Arkansas graben may mark the onset of rifting there. It has been argued that the current configuration of the rift began ca. 21 Ma (Ingersoll, 2001), consistent with the initiation of major rift opening (Ricketts et al., 2015).

Apatite fission-track cooling ages from some fault-bounded, rift-margin mountain ranges (Kelley et al., 1992; Kelley and Chapin, 1995; House et al., 2003; Ricketts et al., 2015) indicate that rift-flank uplift associated with rift opening has occurred since the late Oligocene, consistent with up to 6 km of Oligocene–Quaternary basin fill in adjoining rift basins, such as the Albuquerque Basin (Grauch and Connell, 2013) and northern San Luis Basin (Kluth and Schaftenaar, 1994). Despite this long duration of rift opening, the amount of cumulative crustal stretching in the rift zone is limited. Kluth and Schaftenaar (1994) reported 8%–12% extension across the central San Luis Basin, corresponding to ~4.5–6.5 km of net extension along their seismic line 2, which is ~55 km long. Russell and Snelson (1994) reported 17% and 28%–30% extension in the northern and southern Albuquerque Basin, respectively, corresponding to ~10 km and ~17 km of net extension, respectively (their figure 11). Presumably, net extension is higher in the southern rift zone, where the rift is several basins wide.

The cause of Rio Grande rift initiation has been debated for decades. Lucas and Ingersoll (1981) proposed that plate-boundary reorganizations along the North American west coast were responsible for an extensional stress regime in the western United States, facilitating Rio Grande rift opening. Voluminous magmatism that preceded the onset of Rio Grande rift extension may have weakened the lithosphere (e.g., Baldridge et al., 1995). The upper mantle plays an important role as a driving force for rift opening in recent studies (van Wijk et al., 2008; Karlstrom et al., 2012; Ricketts et al., 2015; Ricketts and Karlstrom, 2016). Indeed, van Wijk et al. (2008) proposed that Farallon slab foundering exposed a step in the lithosphere-asthenosphere boundary that led to small-scale mantle convection and localized rift opening west of the Great Plains. Ricketts et al. (2015) and Ricketts and Karlstrom (2016) proposed that rift opening was the direct result of Farallon slab rollback and foundering (Bird, 1984), which created a gap in the sinking Farallon plate (Liu and Currie, 2016) that focused mantle upwelling. Moucha et al. (2008) suggested that whole-mantle flow caused rift opening. Mantle buoyancy may have contributed to a more recent (post–10 to 6 Ma) phase of uplift north of the Rio Grande region (Southern Rocky Mountains; Karlstrom et al., 2012) and around the Jemez Lineament since ca. 5 Ma (Nereson et al., 2013; Repasch et al., 2017).

Middle–Late Quaternary Rift Opening

The middle–late Quaternary tectonic activity of the Rio Grande rift (a time period for which no tectonic subsidence analysis is available) is summarized here. Figure 2 shows the distribution of well-studied Quaternary faults in New Mexico (Machette et al., 1998; note that Machette et al. [1998] used the older Quaternary age span of 1.6–0 Ma). Sixteen rift faults have received close study.

The locations of these faults and various paleoseismic parameters (e.g., age of most recent surface rupture, recurrence interval, slip rates, vertical displacement per event) are listed in Table 1 and illustrated in Figure 3. Inspection of Figures 2 and 3 indicates that the proportion of extensional strain on the master fault versus distributed intrabasinal faults changes from basin to basin. Quaternary faulting appears to be well distributed in the northern Albuquerque Basin (Albuquerque area). However, in the Española Basin, the only verified Pleistocene surface ruptures are along the master fault system (i.e., the Pajarito-Embudo fault system). In the southern San Luis Basin, late Pleistocene faulting is generally concentrated on the Sangre de Cristo fault, a mountain-front fault zone on the eastern side of the basin. The apparent distribution of young faulting is partly dependent on the age of preserved geomorphic surfaces within a given basin. Specifically, older surfaces will preserve more surface ruptures (e.g., the 0.8 Ma Cuchillo surface in the Palomas Basin [McCraw and Love, 2012] and the 1.5 Ma Llano de Albuquerque surface in the western Albuquerque Basin [Connell et al., 2013]), but basins with younger surfaces would be expected to have fewer fault scarps, such as Tularosa Basin, the floor of which is mostly latest Pleistocene or Holocene in age (Love et al., 2012). However, the Española Basin and the southern San Luis Basin contain sufficient older surfaces (i.e., terrace deposits in the Española Basin and basalt-capped highlands in the southern San Luis Basin) to record middle–late Quaternary surface-rupture events. This distribution of deformation in the Rio Grande rift fits the typical evolution of narrow continental rift zones, where later stages of stretching and rift opening are characterized by activation of intrabasinal faults (Corti, 2008, 2012; Beutel et al., 2010; Ricketts et al., 2014).

Quaternary paleoseismicity of the Rio Grande rift (Table 1) is characterized by low rates of slip (<0.2 mm/yr, but commonly 0.01–0.02 mm/yr) on most faults, and recurrence intervals between large earthquakes on individual faults (M 6.25–7.5) are commonly on the scale of tens of thousands of years, with most faults having recurrence intervals of 50–250 k.y. (Machette et al., 1998; Personius et al., 1999; Table 1). Frequent small earthquakes (up to M 5 and occasionally M 6) have occurred across New Mexico (see Sanford et al., 2002, their figures 1 and 2), as represented by the historical seismic record, but these typically cannot be attributed to slip on mapped Rio Grande rift faults. However, known Quaternary fault scarps (Machette et al., 1998) clearly are associated with the Rio Grande rift. The estimated minimum recurrence interval of strong (M > 6.5), surface-rupturing earthquakes averaged over the rift is once every 400–1000 yr (Machette et al., 1998; Wong et al., 2004).

Direct evidence for Quaternary extension was provided by Ricketts et al. (2014), who documented high local Quaternary strain rates on the western margin of the Albuquerque Basin. Quaternary strain rates calculated from vein opening in travertine deposits are an order of magnitude larger than the Oligocene–present strain rates of Rio Grande rift opening (Ricketts et al., 2014). These opening rates are two orders of magnitude larger than global positioning system (GPS) measurements analyzed by Murray et al. (2015). Thus, rift opening rate varies with the time scales of processes involved (Ebinger et al., 2013).

Miocene-Pliocene Unconformity

Lateral Extent and Character

The Miocene-Pliocene unconformity was first described in the 1930s along the margins of the asymmetric basins of the Rio Grande rift, and it has since been recognized across most of Española Basin (Fig. 2; Bryan, 1938; Bryan and McCann, 1938; Wright, 1946; Stearns, 1953, 1979; Seager et al., 1984; Connell et al., 2013; Koning et al., 2013, 2016a; Chamberlin et al., 2016), and more recently, outside of the rift zone (for example, Ocate volcanic field east of the rift; O'Neill, 1998; Nereson et al., 2013). In the rift, the unconformity has been documented from the Arkansas Basin in Colorado to the Rincon Basin in southern New Mexico. It is not described in central-basin depocenters (Fig. 2); if the tectonic subsidence rate as a result of rift opening or slip on a fault exceeds a regional epeirogenic uplift rate, the net effect is still subsidence (probably at a lower rate), and no unconformity is recorded. Where exposed in the rift, the Miocene-Pliocene unconformity has been described as an angular unconformity with dip discordance typically reaching 10°–20°, and locally as much as 32° (e.g., Connell et al., 2013). Figure 2 shows our compilation of the locations where the unconformity has been identified in field studies in or near the Rio Grande rift. Table 2 lists a detailed description and sources that were used to construct the compilation.

In the northernmost rift basins, the unconformity has been observed to span the Arkansas Basin (north of the San Luis Basin) and the structural high between the Arkansas and San Luis Basins (the Poncha Pass area; S. Minor, 2016, personal commun.). It is not interpreted in field studies in the northern San Luis Basin (Alamosa area; Fig. 2). The unconformity has been mapped along the southwestern margin of the San Luis Basin (Koning et al., 2016a). It was observed there only on the distal hanging wall opposite of the master fault system. The spatial extent of the unconformity in the central San Luis Basin is unknown, since it is covered by the Servilleta Basalt. On the southwest margin of this basin, the unconformity is overlain by basalts that have been dated ca. 5.5–4.8 Ma (Tables 2–4).

The timing of the unconformity in the central/southern San Luis Basin partly overlaps with inferred southward river integration of the ancestral Rio Grande between 5.5 and 4.5 Ma (Mack et al., 1998, 2006; Connell et al., 2005; Koning et al., 2016b; Repasch et al., 2017).

The unconformity is particularly extensive in the Española Basin, where it covers >90% of the basin's area, if one interpolates between areas of preservation (Galusha and Blick, 1971; Spiegel and Baldwin, 1963; Manley, 1979; Baldridge et al., 1994; Koning et al., 2013), and it is absent only in restricted depocenters immediately adjacent to the Pajarito fault system (Fig. 2). Outcrop and well data in the Española Basin generally show a sharp lithologic change across the contact corresponding with the unconformity. In the north-central portion of the basin, the unconformity is overlain by basalts that have been dated at 4.9–3.3 Ma (Koning et al., 2011, 2013; Maldonado et al., 2013; Repasch et al., 2017). Underlying strata range from 10 Ma to 6 Ma (Table 2; Koning et al.,

TABLE 2. DATA REGARDING UNCONFORMITY AGE AND SPATIAL EXTENT

Basin	Intrabasin location	Notes and references
San Luis Basin	Central part	Unconformity extent unknown because of cover by Servilleta Basalt. Drawn around southwest margins of Timber Mountain horst and the structural high under the San Luis Hills, the boundaries of which were interpreted using geophysical interpretations (Grauch et al., 2004, 2017; Drenth et al., 2013) and geologic mapping (Thompson et al., 2015).
	Southwest margin	Unconformity mapped by Koning et al. (2007a, 2007b) and Aby (2008). Three overlying basalts (ca. 5.5 Ma and ca. 4.8 Ma) dated (Koning et al., 2016a; Repasch et al., 2017). Age of overlying basalt elsewhere is 4.8 Ma (Appelt, 1998).
Española Basin	North-central	Well exposed under Black Mesa and La Mesita (mapped by Koning and Aby, 2003; Koning and Manley, 2003; Koning, 2004). Overlying basalts dated using Ar/Ar technique at 4.5–3.5 Ma (Koning et al., 2011, 2013; Maldonado et al., 2013; Repasch et al., 2017); underlying Ojo Caliente Sandstone interpreted to be 9–10 Ma (Koning et al., 2011; Repasch et al., 2017).
	Northeast	Mapped under thin veneer of Pliocene–Pleistocene gravel at various geomorphic levels (Manley, 1979; Smith et al., 2002; Bauer et al., 2005). Highest geomorphic level projects under a 4.8 Ma basalt on La Mesita (Koning et al., 2013).
	Southeast	Underlies the Ancha Formation and the Cerros del Rio basalts (Koning et al., 2002; Koning and Read, 2010).
	South-central	Mapped under Puye Formation west of Rio Grande (Galusha and Blick, 1971; Dethier, 2003; Koning and Read, 2010). Exposed in Bayo Canyon and overlain by a 5.3 Ma vitric ash and 8.8 Ma basalt (WoldeGabriel et al., 2001). In well data, interpreted to be underlain locally by basalts (average age of 8.5 Ma per WoldeGabriel et al., 2001, 2013; Broxton et al., 2001) or 7.0–6.8 Ma Bearhead Rhyolite tephra (Broxton et al., 2012). Subsurface extent drawn using Cole et al. (2009).
Albuquerque Basin	Northwest	Boundary drawn using compilation map by Connell (2008a); subsurface extent slightly modified from Connell et al. (2013). Age control given by underlying Peralta Tuff and 6.5 Ma clast ages (Connell, 2008a, 2008b) as well as magnetostratigraphy (Connell et al., 2013).
	Western margin	Boundary drawn using Maldonado et al. (2007), New Mexico Bureau of Geology and Mineral Resources (2003), and Lozinsky and Tedford (1991).
	Southwest	Boundary drawn using Machette (1978) and New Mexico Bureau of Geology and Mineral Resources (2003).
	Southeast	Not exposed, but subsurface extent was inferred to underlie structural benches (Connell et al., 2013).
	Northeast	Not exposed, but subsurface extent was inferred to underlie structural benches (Connell et al., 2013).
	North-central	Stratigraphic sequence appears conformable (Smith et al., 2001; Smith and Kuhle, 1998); locally, a disconformity has been inferred just below the 7.0–6.7 Ma Peralta Tuff (Chamberlin et al., 1999).
Socorro Basin	Eastern margin	Unconformity locally exposed (Cather et al., 2004).
La Jencia Basin	Northeast	Noted in mapping by Cather and Read (2003). Overlain by 3.2 Ma travertine (Lueth et al., 2016).
	Southeast	Inferred to lie under coarse Pliocene–Pleistocene deposits (Chamberlin and Osburn, 2006; Chamberlin, 2004).
San Marcial and Engle Basins		Not reported to be exposed (e.g., Cikoski and Koning, 2013; Cikoski et al., 2017).
Winston Basin		Unconformity interpreted and mapped by Koning (2012) and Harrison and Cikoski (2012). Age of overlying basalt (4.9 Ma) from McLemore et al. (2012).
Palomas Basin	Western margin	Generally gradational through most of basin, but angular unconformity interpreted in some westernmost exposures (Jochems, 2015; Jochems and Koning, 2016; Koning et al., 2015; Jochems and Koning, 2017).
	Southwest	Unconformity south of Tierra Blanca Creek (Jochems, 2017).
	Near Truth or Consequences	Local disconformities but largely gradational (Jochems and Koning, 2015; Koning et al., 2016b; Andrew Jochems, 23 June 2017, written commun.).
Hatch-Rincon Basin		Where not eroded, an angular unconformity is widespread (Seager and Hawley, 1973; Seager et al., 1975; Seager and Mack, 1991, 2003).
Mesilla Basin	Northernmost part; structural high to north	Unconformity recognized and mapped by Seager et al. (1971, 1975).
Tularosa Basin	Northeast	A likely unconformity inferred in one locale between Pliocene–Pleistocene strata and older, more tilted strata (Koning, 2009). Otherwise, the Pliocene-Miocene unconformity has not been noted in the Tularosa Basin.

2011, 2013; Repasch et al., 2017). In the northeast, the unconformity has been mapped below a thin gravel layer occupying various geomorphic levels. In the southeast, the unconformity underlies the Ancha Formation (Table 2) and the 2.7–2.2 Ma Cerros del Rio basalts (Thompson et al., 2006; Koning et al., 2002; Koning and Read, 2010). Dating of strata across the unconformity 4–5 km east of Los Alamos, on a structural high (Cole et al., 2009; Koning et al., 2013), demonstrated that a 5.3 Ma vitric ash lies above the contact, and 8.8 Ma basaltic lavas lie below it (Bayo Canyon locality; WoldeGabriel et al., 2001, 2013). The wide extent of the unconformity in this basin may be due to widespread erosion and exposure of the basin due to Pliocene–Pleistocene uplift along the La Bajada fault to the south. Additionally, widespread erosion may have been promoted in the central Española Basin due to the Picuris-Pecos fault facilitating tilting of the distal hanging wall, resulting in a doubly north- and south-plunging block (Smith and Roy, 2001; Smith, 2004).

In the Albuquerque Basin, the unconformity has been described on both western and eastern margins of the basin (Maldonado et al., 2007; Connell,

TABLE 3. WELL DATA K3, SAN LUIS BASIN

Lithologic unit	Top (km)	Base (km)	Age top (Ma)	Age base (Ma)	ρ	*C*	φ_0	Data source
Upper basalt flow of Servilleta Formation (Tusb)	0.073	0.088	3.0	3.6	2795	0.01	0.0	b, c, d, j
Strata between the upper and middle basalt flows of the Servilleta Formation (Tusb & Tmsb)	0.088	0.112	3.6	4.0	2170	0.27	0.35	b, c, d, j
Middle Servilleta Formation basalt flow (Tmsb)	0.112	0.127	4.0	4.0	2795	0.01	0.0	b, c, d, j
Strata between the lower and middle basalt flows of the Servilleta Formation (Tmsb & Tlsb)	0.127	0.173	4.0	4.7	2170	0.27	0.35	b, c, d, j
Lower Servilleta Formation basalt flow (Tlsb)	0.173	0.213	4.7	4.8	2795	0.01	0.0	b, c, d, j
Chamita Formation	0.213	0.32	4.8	9.0	2170	0.22	0.33	b, c, d
Ojo Caliente Sandstone Member, Tesuque Formation	0.32	0.533	9.0	13.5	2170	0.27	0.4	b, c, d, h, i

Note: ρ—density (kg/m^3), *C*—porosity-depth coefficient, φ_0—porosity at surface. Data sources: b—Drenth et al. (2013), c—Rowan et al. (2003), d—Drakos et al. (2004), h—Koning et al. (2011); i—Koning et al. (2013), j—Appelt (1998).

2008a; Connell et al., 2013; and others; see Table 2), and it has not been documented in the central depocenter. The Pliocene Ceja Formation overlies the erosional paleosurface on the western margin (Connell et al., 2013). On the eastern margin, the unconformity is inferred in the subsurface on the footwalls of major faults (Connell et al., 2013). In the northern Albuquerque Basin (i.e., the Santo Domingo subbasin), the stratigraphic sequence appears conformable (Smith et al., 2001; Smith and Kuhle, 1998); locally, a disconformity has been inferred just below the 7.0–6.7 Ma Peralta Tuff (Chamberlin et al., 1999). Associated erosional surfaces have developed on prerift bedrock both west and east of the northern Albuquerque Basin (Bryan and McCann, 1938; Wright, 1946; Stearns, 1953, 1979), as discussed later herein.

South of the Albuquerque Basin, playa deposits are restricted to below the unconformity (except for basins that have remained endorheic), and, near basin axes, fluvial deposits associated with a southward-extending Rio Grande River overlie this contact (Mack et al., 1994b; Connell et al., 2005). The lacuna of the unconformity spans anywhere between 8.8 and 6 Ma (onset) and 5.3–3.0 Ma in the wells and stratigraphic columns discussed in the next section, depending on location and structural position within a given basin. Age control in the Albuquerque, La Jencia, Socorro, and Palomas Basins indicates that the associated lacuna generally spans 6.8–5.0 Ma (Table 2; Seager et al., 1984; Chamberlin et al., 1999; Chamberlin and Osburn, 2006; Koning et al., 2015), and possibly as young as 3 Ma near the western and southwestern margins of the Albuquerque Basin (Table 2; Connell et al., 2013; Chamberlin et al., 2016).

In the southern rift, the unconformity is most notable on the footwall of the Socorro fault zone (eastern La Jencia Basin), near the western margin of the Palomas Basin, and in and near the Rincon Basin. The latter, which lies between the deeper Palomas and Mesilla Basins, experienced a reconfiguration of faulting between 8 and 5 Ma and widespread erosion (Mack et al., 1994b).

TABLE 4. WELL DATA AIRPORT WELL, SAN LUIS BASIN

Lithologic unit	Top (km)	Base (km)	Age top (Ma)	Age base (Ma)	ρ	*C*	φ_0	Data source
Blueberry Hill or Lama Formation	0	0.013	0.5	3.1	2170	0.01	0.0	b, c, d
Upper basalt flow of Servilleta Formation (Tusb-upper)	0.013	0.024	3.1	3.1	2795	0.01	0.0	b, c, d, j
Strata between Tusb-upper basalt flow and Tusb-lower basalt flow of the Servilleta Formation	0.024	0.034	3.1	3.6	2170	0.27	0.35	b, c, d, j
Lower upper basalt flow of the Servilleta Formation (Tusb-lower)	0.034	0.044	3.6	3.6	2795	0.01	0.0	b, c, d, j
Strata between the lower upper flow (Tusb-lower) and middle basalt flows of the Servilleta Formation	0.044	0.065	3.6	4.0	2170	0.27	0.35	b, c, d, j
Middle Servilleta Formation basalt flow (Tmsb)	0.065	0.137	4.0	4.0	2795	0.01	0.0	b, c, d, j
Strata between the lower and middle basalt flows of the Servilleta Formation (Tmsb & Tlsb)	0.137	0.148	4.0	4.7	2170	0.27	0.35	b, c, d, j
Lower Servilleta Formation basalt flow (Tlsb)	0.148	0.152	4.7	4.8	2795	0.01	0.0	b, c, d, j
Chamita Formation	0.152	0.21	4.8	9.0	2170	0.22	0.32	b, c, d
Ojo Caliente Sandstone Member, Tesuque Formation	0.21	0.52	9.0	13.5	2170	0.27	0.4	b, c, d, h, i

Note: ρ—density (kg/m^3), *C*—porosity-depth coefficient, φ_0—porosity at surface. Data sources: b—Drenth et al. (2013), c—Rowan et al. (2003), d—Drakos et al. (2004), h—Koning et al. (2011); i—Koning et al. (2013), j—Appelt (1998).

Similarly, a displacement rate increase or concentration (from nearby faults) of extensional strain likely occurred along the Socorro fault zone beginning ca. 7 Ma, based on a footwall stratigraphic unit that likely predates major movement along the fault (Tpfp of Chamberlin et al., 1999; R. Chamberlin, 2016, written commun.).

Outside of the rift zone, an unconformity (corresponding to a high-level geomorphic surface that could be termed a peneplain) lies buried beneath volcanic rocks in the Mount Taylor region (Fig. 2, purple, northwest of ABQ; Bryan and McCann, 1938; Wright, 1946; Stearns, 1953, 1979). Because it is overlain there by relatively young basalt flows (4.5–2.5 Ma, mostly 3.2–2.5 Ma; Hallett, 1994; Hallett et al., 1997; Crumpler, 1982; Dunbar, 2005), it would be younger than the majority of the lacuna in the rift. For this reason, we are not certain that this unconformity can be related to the Miocene-Pliocene unconformity in the rift. Erosional surfaces in the Ocate volcanic field, east of the rift zone, are dated at 8.3–5.5 Ma (highest erosional surface) and 5.0–4.0 Ma (intermediate erosional surface; O'Neill, 1998; Stroud, 1997; Olmsted and McIntosh, 2004; Nereson et al., 2013), and they temporally overlap the rift unconformity; for this reason, we correlate this unconformity with the rift unconformity.

Existing Models for the Miocene-Pliocene Unconformity

Previous models explaining the formation of the unconformity in the Rio Grande rift generally have invoked changing tectonism, mantle upwelling, or climate-modulated sediment supply. Bryan (1938) interpreted that the unconformity formed during one or more prolonged periods of erosion concomitant with stabilized stream grades, which occurred after tectonism associated with rift-flank uplifts. Cather et al. (1994) interpreted the unconformity to be a result of rapid tectonism and basin tilting in the late Miocene. In this scenario, the creation of accommodation space exceeded the sediment supply rate in the late Miocene, which caused offlap of sedimentation into narrow areas of maximum basin subsidence and widespread erosion of older sediments on the distal hanging walls. This explanation for the lacuna would be applicable to the margins of the rift basins. Early Pliocene onlap of postunconformity sediment toward the basin margins would reflect a waning of tectonism following the lacuna associated with the unconformity (Cather et al., 1994), consistent with the fact that the upper sedimentary package has undergone only minor deformation. This unconformity model is not robustly supported by existing tilt data sets; for example, Cather et al. (1994, their figure 3) and Koning et al. (2013) showed that most stratal tilt change occurred between 16 and 10 Ma, rather than later in the late Miocene. A major climate change affected the southwestern United States between 7 and 5 Ma, during which opening of the Gulf of California (Oskin and Stock, 2003) intensified the North American monsoon and resulted in fluvial integration of endorheic basins (Chapin, 2008). Climate-modulated sediment supply changes that occurred during waning or constant tectonic subsidence have been explicitly invoked to explain the Miocene-Pliocene unconformity in the Albuquerque Basin (Connell et al., 2013).

Tilting of the Ogallala Formation, Western Great Plains

Uplift of the eastern edge of the Southern Rocky Mountains, by as much as 1 km, has caused eastward tilting of the Ogallala Formation since the late Miocene (Steven et al., 1997; McMillan et al., 2002, 2006; Leonard et al., 2002; Duller et al., 2012). The tilting has been quantified in northeast New Mexico, Colorado, and farther north (Cather et al., 2012, and references therein; Duller et al., 2012). The Ogallala Formation in southeastern New Mexico (i.e., the part that is bounded on the west by the Mescalero Ridge) is almost entirely eolian, and paleogradients (and therefore tilting) have not been estimated. Duller et al. (2012) found that in the central Great Plains, tilting may have occurred ca. 6–3.7 Ma.

Many studies have attributed tilting of the Ogallala Formation and the western Great Plains to dynamic (mantle driven) uplift; related to the Jemez Lineament (Nereson et al., 2013), centered in the Southern Rocky Mountains (McMillan et al., 2006); or northward propagation of the Rio Grande rift (Duller et al., 2012). Other studies have pointed to tectonic rock uplift related to Rio Grande rift opening (Steven et al., 1997; Leonard et al., 2002), isostatic rock uplift as a result of erosion (Leonard et al., 2002), climate effects (Duller et al., 2012; Nereson et al., 2013), and crustal heating (Eaton, 2008).

BACKSTRIPPING ANALYSIS OF MIDDLE MIOCENE TO PRESENT SUBSIDENCE HISTORY OF THE RIO GRANDE RIFT

The opening history of the Rio Grande rift has been inferred from stratigraphic and structural field studies (e.g., tilting rates or thickness changes; Chamberlin, 1983; Cather et al., 1994; Koning et al., 2013; Smith et al., 2002), sparse tectonic subsidence analyses (Connell et al., 2013; Grauch and Connell, 2013), and thermochronologic studies of rift-flank uplift (Kelley et al., 1992; House et al., 2003; Ricketts et al., 2015). These studies suggest that the rift opened rapidly starting ca. 24–20 Ma (Ricketts et al., 2015), and the loci of extensional strain shifted spatially with time (Baldridge et al., 1994; Koning et al., 2013; Grauch and Connell, 2013).

We present tectonic subsidence histories of four major Rio Grande rift basins: San Luis, Albuquerque, Española, and northern La Jencia Basins, using wells and measured sections from 11 locations (Fig. 3). Descriptions of stratigraphy, age constraints, and methods are provided below and in Tables 3–13.

Methods: Tectonic Subsidence Analysis by Backstripping

Tectonic subsidence analysis allows both inter- and intrabasin comparisons of subsidence rates in the rift, which are important for understanding the rift's evolution. However, the subsidence history at any location may be controlled by slip histories of nearby faults and may not be representative of the entire basin. Also, both subsidence and subsidence rates in half graben structures are expected to be spatially variable, i.e., higher on the fault-bounded side and near the centers of master faults, but lower on the hinged side of half grabens, near the ends of master faults, and in accommodation zones.

Tectonic subsidence was calculated using the backstripping method (van Hinte, 1978; Bond and Kominz, 1984) assuming Airy isostasy. In backstripping, unconformities are treated as periods of zero tectonic subsidence (horizontal line segments in Fig. 4). In reality, most unconformities record periods of erosion, which may be promoted during tectonic stability or uplift, but which may record subsidence if erosion rates are faster than subsidence rates. The widespread Miocene-Pliocene unconformity in the Rio Grande rift is erosional in most places, so the rocks below the unconformity are older than the onset of erosion, and there is no record of the actual time that erosion began. In contrast, the age of strata immediately overlying an unconformity gives the onset of renewed deposition.

Using the backstripping method (van Hinte, 1978; Bond and Kominz, 1984), we calculated tectonic subsidence curves from stratigraphic columns. In Figure 4, plotted tectonic subsidence curves show the vertical movements of stratigraphic horizons with respect to the top of each stratigraphic column. We present graphs of the sediment accumulation through time (burial history curves, Fig. 4), and graphs where the burial history curves are corrected for the mechanical compaction and loading that occurs during burial (tectonic subsidence, Fig. 4). Because the Rio Grande rift was not covered by a sea during its opening history, we do not need to correct for sea level or paleobathymetry (Bond and Kominz, 1984). The tectonic subsidence curves represent subsidence as a result of tectonic and dynamic processes, and thus they provide a means of analyzing processes that played a role during rift opening.

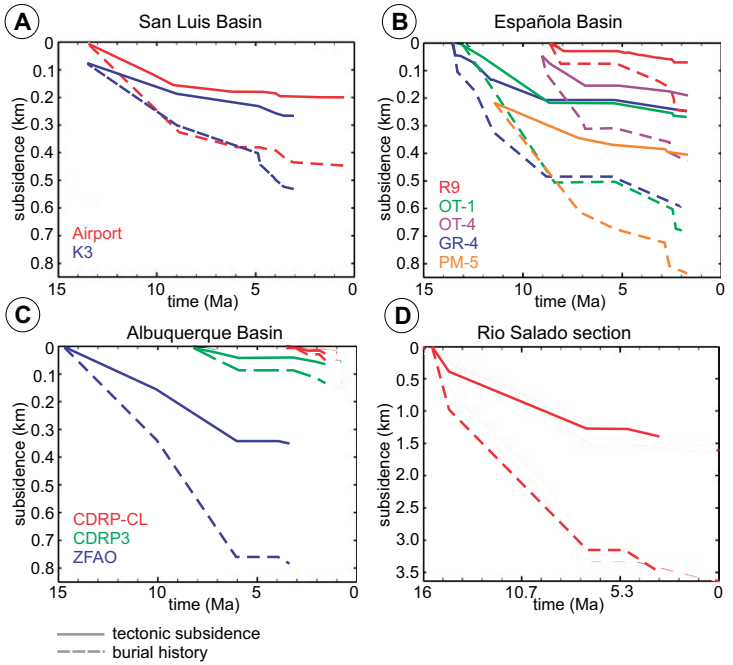

Figure 4. Tectonic subsidence and burial history curves for 10 sites indicated in Figure 3, with data listed in Tables 3–12. (A) San Luis Basin, (B) Española Basin, (C) Albuquerque Basin, (D) Rio Salado section. Note that part D has a different horizontal and vertical scale.

In many of our stratigraphic columns (Tables 3–13; Fig. 5), layers of extrusive rocks (generally basalts) are present. These layers are assigned zero porosity (Tables 3–13) and thus do not undergo decompaction during backstripping. Figure 5 shows an example of a stratigraphic column with interbedded basalt layers for one of the wells that we analyzed (GR-4, Española Basin) and its corresponding burial history curve.

Errors in tectonic subsidence analyses stem from uncertainties in the data sets (such as age of formations). In our analyses, we aimed to reduce errors as much as possible by only using well data/stratigraphic columns for which we had enough age constraints, and we only backstripped the (upper) portion of the columns for which the age constraints were acceptable. As a result, we rejected many wells and deeper portions of other wells.

We show tectonic subsidence curves for two places in the southern San Luis Basin (Tables 3 and 4), five in the Española Basin (Tables 5–9), three in the Albuquerque Basin (Tables 10–12), and one (Table 13) along Rio Salado between the Lemitar Mountains and Sierra Ladrones (Figs. 3, 4, and 5). The latter lies on a west-tilted half graben in the northeastern La Jencia Basin (Cather and Read, 2003). Data used for six of these are from wells, four are from measured stratigraphic sections (Albuquerque Basin and its southwest margin), and one is from a cross section across the northeastern La Jencia Basin (Cather and Read, 2003). More well data and measured sections are available, but, as discussed above, we selected only sites with good age control. The subsurface units were differentiated based on age control and lithologic contrasts.

Parameters used in subsidence modeling (compaction coefficients, surface porosities, and bulk densities) were obtained from published compilations for similar lithologies (McWhorter and Sunada, 1977; Drenth et al., 2013; Rowan et al., 2003) and are listed in Tables 3–13. The Rio Grande rift is in a continental setting, so sea-level change and water depth were assigned zero values. Mantle and water densities used were 3300 kg/m^3 and 1000 kg/m^3, respectively. Errors in parameter values introduce error into the calculations, but we tested ranges of values and found that even substantial changes in parameter values only slightly affected the subsidence curves.

Age Constraints and Model Input

The stratigraphy is relatively unambiguous in the chosen sites (Figs. 3 and 5), and sufficient age control exists to calculate sediment accumulation rates (age control is listed in Tables 2–13). The duration of the Miocene-Pliocene lacuna is relatively well constrained at some sites, because either dateable units are found above and below the unconformity, or the locality is near outcrops with age control (e.g., wells OT-1 and GR-4). In other places, the lacuna duration is constrained by extrapolation of sediment accumulation rates.

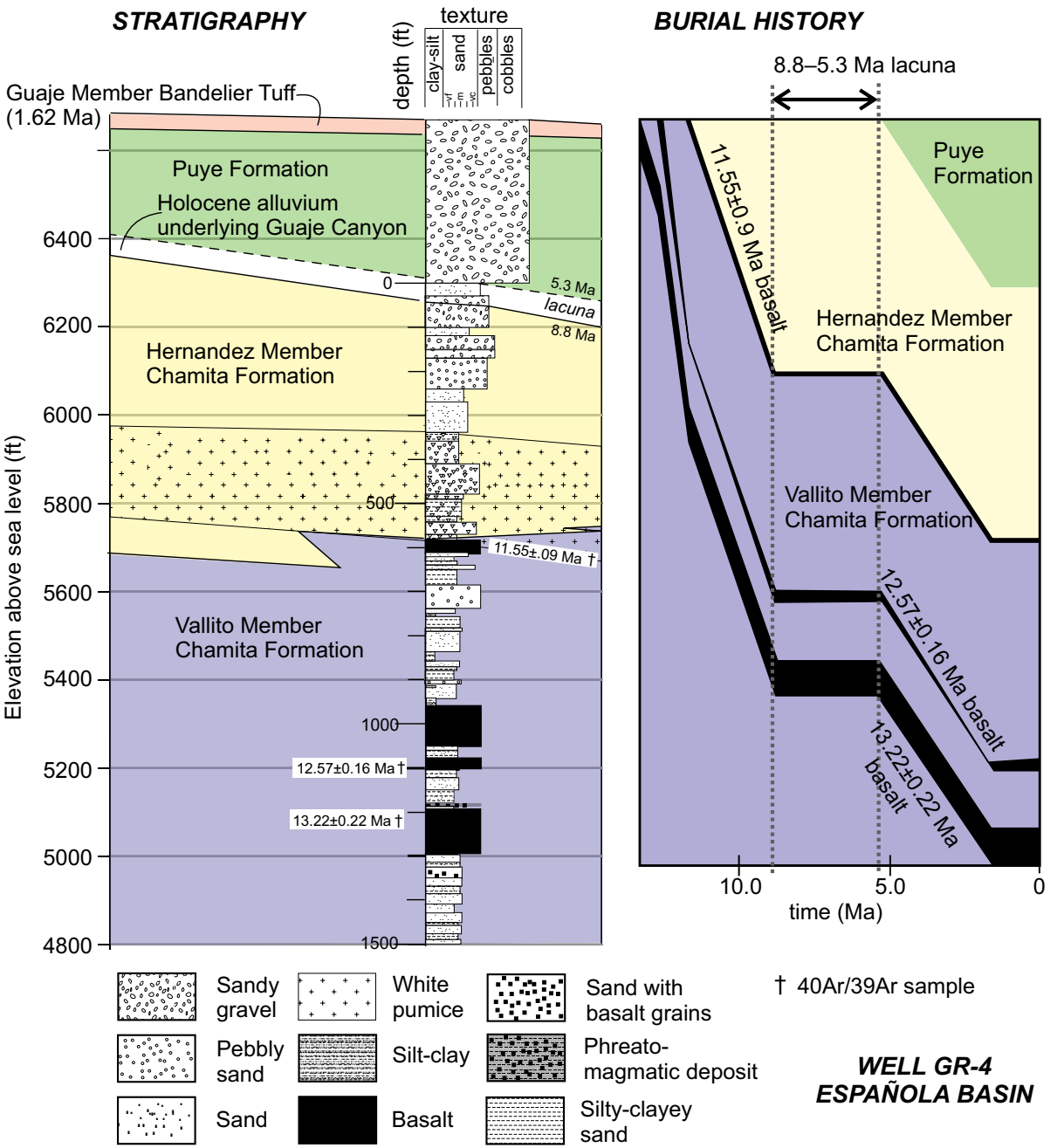

Figure 5. Lithologic diagram of well GR-4 (left) in the Española Basin, and burial history curve (right). Different units of the Santa Fe Group are shown in unique shades. Holocene alluvium in the well was left unshaded. Depth (ft below ground surface) is depicted along left side of stratigraphic column. The lithologic diagram is a modification of Figure 2 of WoldeGabriel et al. (2013). Sand texture grain sizes vary from very fine (vf) through medium (m) to very coarse (vc). The burial history curve was created with Petromod© software.

TABLE 5. WELL DATA GR-4, ESPAÑOLA BASIN

Lithologic unit	Top (km)	Base (km)	Age top (Ma)	Age base (Ma)	ρ	*C*	φ_0	Data source
Puye Formation below Otowi Member of Bandelier Tuff (extends up the slope from well head)	0.0	0.115	1.62*	5.3†	2170	0.15	0.1	b, c, f
Inferred age range of Miocene-Pliocene lacuna	0.115	0.115	5.3†	8.8§	0	0	0	g
Hernandez Member above upper basalt	0.115	0.289	8.8§	11.6	2170	0.2	0.35	b, c, f
Upper basalt in well	0.289	0.295	11.6	11.6	2795	0.01	0.0	b, c, f
Vallito Member between middle and upper basalts in well	0.295	0.438	11.6	12.6	2170	0.29	0.3	b, c, f
Middle basalt in well	0.438	0.445	12.6	12.6	2795	0.01	0	b, c, f
Vallito Member between lower and middle basalt in well.	0.445	0.485	12.6	13.2	2170	0.29	0.38	b, c, f
Lowest basalt in well	0.485	0.509	13.2	13.2	2795	0.01	3.0	b, c, f

Note: ρ—density (kg/m^3), *C*—porosity-depth coefficient, φ_0—porosity at surface. Data sources: b—Drenth et al. (2013), c—Rowan et al. (2003), f—WoldeGabriel et al. (2013), g—WoldeGabriel et al. (2001).

*Age of Otowi Member of Bandelier Tuff (Izett and Obradovich, 1994; Spell et al., 1996a, 1996b).

†Minimum age of Miocene-Pliocene lacuna is from vitric ash immediately overlying the unconformity in Bayo Canyon, located 3.5 km to SSE (WoldeGabriel et al., 2001).

§Maximum age of Miocene-Pliocene lacuna is from dated basalts in Bayo Canyon, located 3.5 km to SSE; these immediately underlie the unconformity (WoldeGabriel et al., 2001).

Age control is from published $^{40}Ar/^{39}Ar$, K/Ar, and paleomagnetic reversal data (Appelt, 1998; Broxton et al., 2001, 2012; Cather and Read, 2003; Chamberlin, 2004; Connell, 2008b; Connell et al., 2013; Drakos et al., 2004; Izett and Obradovich, 1994; Koning et al., 2011, 2013; Spell et al., 1996a, 1996b; WoldeGabriel et al., 2001, 2013). Tests show that errors or uncertainties in the ages are smaller than the sensitivity of the backstripping method and do not change any of our conclusions. A single age was used for subsurface basalt intervals unless more than one age was available. Although it varies spatially, in most locations, the age of the lacuna includes the time period of 7–5 Ma (Tables 3–13).

In the San Luis Basin, the age of the Ojo Caliente Sandstone was taken from the northern Española Basin, where the base and top, respectively, are interpreted to be 13.5 Ma (Koning et al., 2013) and 9 Ma (Koning et al., 2011; Repasch et al., 2017). The subsurface stratigraphy here consists of interbedded Servilleta Basalts (4.8–3.1 Ma; Appelt, 1998) and clastic sediments underlain by gravel-bearing Chamita Formation, which in turn is underlain by a distinctive eolianite called the Ojo Caliente Sandstone (Tables 3 and 4).

In the Española Basin, the subsurface stratigraphy consists of an upper package of interbedded ignimbrites, lava flows (dacites and basalts), and fanglomerates (Puye Formation) that overlie the Miocene-Pliocene boundary. Below this boundary, a lower stratigraphic package consists of the Chamita Formation interbedded with 13–8 Ma basalts. Details of the subsurface stratigraphy and age control were presented by WoldeGabriel et al. (2006, 2013).

TABLE 6. WELL DATA OT-1, ESPAÑOLA BASIN

Lithologic unit	Top (km)	Base (km)	Age top (Ma)	Age base (Ma)	ρ	*C*	φ_0	Data source
Stratigraphic interval between uppermost basalt (Tb4) and Otowi Member of Bandelier Tuff in exposed slopes above well head	0.0	0.015	1.6*	2.1†	2170	0.15	0.1	b, c, f
Age range of Tb4 lava flows	0.015	0.085	2.1†	2.5†	2795	0.01	0	b, c, f
Puye Formation between uppermost basalt (Tb4) and Miocene-Pliocene unconformity above Tb2	0.085	0.189	2.5†	5.3§	2170	0.15	0.1	b, c, f
Age range of Miocene-Pliocene lacuna	0.189	0.189	5.3§	8.5#	0	0	0	g
Upper basalt (Tb2)	0.189	0.213	8.5#	8.5#	2795	0.01	0.0	b, c, f
Chamita Formation between lower (Tb1) and middle (Tb2) basalts	0.213	0.68	8.5#	13.2	2170	0.22	0.32	b, c, f
Lower basalt (Tb1)	0.68	0.686	13.2	13.2	2795	0.01	0.0	b, c, f

Note: ρ—density (kg/m^3), *C*—porosity-depth coefficient, φ_0—porosity at surface. Data sources: b—Drenth et al. (2013), c—Rowan et al. (2003), f—WoldeGabriel et al. (2013), g—WoldeGabriel et al. (2001).

*Age of Otowi Member of Bandelier Tuff (Izett and Obradovich, 1994; Spell et al., 1996a, 1996b).

†Age range of Tb4 from D. Broxton (1 July 2016, written commun.), which is extrapolated from available age control in adjacent R-9 well (Broxton et al., 2001).

§Minimum age of Miocene-Pliocene lacuna is from vitric ash immediately overlying the unconformity in Bayo Canyon, located 1.6 km to NNW (WoldeGabriel et al., 2001).

#Average of listed age ranges in WoldeGabriel et al. (2001, 2013) for likely correlative basalts in R-9 (D. Broxton, 1 July 2016, written commun.).

TABLE 7. WELL DATA PM-5, ESPAÑOLA BASIN

Lithologic unit	Top (km)	Base (km)	Age top (Ma)	Age base (Ma)	ρ	*C*	φ_0	Data source
Puye Formation and lavas between volcanic flow (~248 m depth) and base of Otowi Member of Bandelier Tuff	0.221	0.248	1.6	2.5	2480	0.1	0.05*	b, c, f, g
Lowest dated Tvt2 dacite flow (~337 m depth) to higher volcanic flow (~248 m depth)	0.248	0.337	2.5	2.7	2795	0.01	0.0	b, c, f, g
Base of Puye Formation to lowest dated Tvt2 dacite flow (~337 m depth)	0.337	0.387	2.7	5.3†	2170	0.15	0.1	b, c, f, g
Base of pumiceous unit (Tjfp) to base of Puye Formation	0.387	0.448	5.3*	7.0§	2170	0.20	0.2	b, c, f, k
Chamita Formation between base of the pumiceous unit (Tjfp) and the base of lower Miocene basalt (Tb1)	0.448	0.832	7.0§	11.4	2783	0.22	0.32	b, c, f, g

Note: ρ—density (kg/m³), *C*—porosity-depth coefficient, φ_0—porosity at surface. Data sources: b—Drenth et al. (2013), c—Rowan et al. (2003), f—WoldeGabriel et al. (2013), g—WoldeGabriel et al. (2001), k—Broxton et al. (2012).
*Interval consists of subequal proportions of lavas and sediment, so value represents an average of 0 and 0.1.
†Base of Puye Formation is constrained in Bayo Canyon outcrops (WoldeGabriel et al., 2001).
§Age of lower pumiceous unit is 7.0–6.8 Ma; this age and glass compositions indicate correlation with Bearhead Rhyolite (Broxton et al., 2012). Note that the unconformity is not extended de facto to PM-5 because the well is too far from outcrop control.

TABLE 8. WELL DATA OT-4 WELL, ESPAÑOLA BASIN

Lithologic unit	Top (km)	Base (km)	Age top (Ma)	Age base (Ma)	ρ	*C*	φ_0	Data source
Puye Formation, Tb4 basalt flow to base of Otowi Member	0.047	0.079	1.6*	2.5	2170	0.15	0.1	b, c, f, g
Tb4 basalt flow*	0.079	0.118	2.5	2.5	2795	0.01	0	b, c, f, g
Puye Formation base (unconformity) to Tb4 basalt	0.118	0.167	2.5	5.3†	2170	0.15	0.1	b, c, f, g
Age range of Miocene-Pliocene lacuna	0.167	0.167	5.3†	6.8	0	0	0	g, k
Lower pumiceous interval (top is unconformity)	0.167	0.201	6.8§	7.0§	2170	0.20	0.2	b, c, f, k
Chamita Formation between middle of upper Tb2 basalt and base of pumiceous interval	0.201	0.372	7.0	8.8	2170	0.22	0.32	b, c, f, g
Base of lower Tb2 basalt to middle of upper Tb2 basalt	0.372	0.432	8.8	9.0	2480	0.1	0.15	b, c, f, g

Note: ρ—density (kg/m³), *C*—porosity-depth coefficient, φ_0—porosity at surface. Data sources: b—Drenth et al. (2013), c—Rowan et al. (2003), f—WoldeGabriel et al. (2013), g—WoldeGabriel et al. (2001), k—Broxton et al. (2012).
*Age of Otowi Member of Bandelier Tuff (Izett and Obradovich, 1994; Spell et al., 1996a, 1996b).
†Minimum age of Puye Formation (minimum age constraint of lacuna) is from vitric ash immediately overlying the unconformity in Bayo Canyon (WoldeGabriel et al., 2001).
§Age of lower pumiceous unit is 7.0–6.8 Ma; this age and glass compositions indicate correlation with Bearhead Rhyolite (Broxton et al., 2012).

TABLE 9. WELL DATA R-9 WELL, ESPAÑOLA BASIN

Lithologic unit	Top (km)	Base (km)	Age top (Ma)	Age base (Ma)	ρ	*C*	φ_0	Data source
Stratigraphic interval between uppermost basalt (Tb4) and Otowi Member of Bandelier Tuff in exposed slopes above well head	0.0	0.001	1.6*	2.1	2170	0.27	0.31	b, c, f, l
Age range of Tb4 basalts	0.001	0.077	2.1	2.5	2795	0.01	0	b, c, f, l
Puye Formation between base of Puye Formation to base of Tb4 basalts	0.077	0.168	2.5	5.3†	2170	0.25	0.1	b, c, f, l
Chamita Formation between lowest basalt (Tb2) and base of Puye Formation§	0.168	0.213	5.3†	8.5	2170	0.22	0.32	b, c, f, l
Lowest basalt (Tb2)	0.213	0.243	8.5	8.5	2795	0.01	0.0	b, c, f, l

Note: ρ—density (kg/m³), *C*—porosity-depth coefficient, φ_0—porosity at surface. Data sources: b—Drenth et al. (2013), c—Rowan et al. (2003), f—WoldeGabriel et al. (2013), l—Broxton et al. (2001).
*Age of Otowi Member of Bandelier Tuff (Izett and Obradovich, 1994; Spell et al., 1996a, 1996b).
†Minimum age of Puye Formation (minimum age constraint of lacuna) is from vitric ash immediately overlying the unconformity in Bayo Canyon (WoldeGabriel et al., 2001).
§Although an unconformity is likely present, we could not use sedimentation rates to adequately constrain the lacuna in this well. Instead, we modeled a condensed section.

TABLE 10. STRATIGRAPHIC SECTION CDRP3, ALBUQUERQUE BASIN

Lithologic unit	Top (km)	Base (km)	Age top (Ma)	Age base (Ma)	ρ	*C*	φ_0	Data source
Rio Puerco Member below Llano de Albuquerque	0.0	0.021	1.6	1.9	2170	0.2	0.21	a, b, c
Inferred lacuna age range of disconformity between Rio Puerco and Atrisco Member of Ceja Formation	0.021	0.021	1.9	2.0	0	0	0	a
Atrisco Member of Ceja Formation	0.021	0.047	2.0	3.02	2170	0.25	0.29	a, b, c
Inferred lacuna age range of Miocene-Pliocene unconformity	0.047	0.047	3.02	5.9	0	0	0	a
Navajo Draw Member, Arroyo Ojito Formation, between Cerro Colorado dacite and higher Miocene-Pliocene unconformity	0.047	0.093	5.9*	7.16	2170	0.29	0.33	a, b, c
Navajo Draw Member, Arroyo Ojito Formation, between La Mesita flow and higher Cerro Colorado dacite	0.093	0.13	7.16	8.16	2350	0.29	0.33	a, b, c

Note: ρ—density (kg/m³), *C*—porosity-depth coefficient, φ_0—porosity at surface. Data sources: a—Connell et al. (2013), b—Drenth et al. (2013), c—Rowan et al. (2003).
*Indicates age that is extrapolated from stratal accumulation rates calculated from underlying interval.

In the Española Basin, the Miocene-Pliocene unconformity in GR-4 lies 164 m above a 11.6 Ma basalt. Figure 5 shows a stratigraphic column of this well. The lacuna here is not well constrained at the well but is inferred to be similar to that exposed in an illustrative outcrop in Bayo Canyon, located 3 km to the south. There, the unconformity is overlain by a 5.3 Ma vitric tuff and underlain by an 8.8 Ma basalt (WoldeGabriel et al., 2001, 20013). Other wells in the Española Basin lie along an east-west transect ~5.5 km south of GR-4 (Fig. 3). In well PM-5, at the top of the Chamita Formation (pre-unconformity strata), there is a distinctive pumiceous unit, which is interpreted to be 7.0–6.8 Ma based on dating and geochemical correlation with the Bearhead Rhyolite (Broxton et al., 2012). At a depth of 337 m, a dacite flow interbedded within the Puye Formation yielded an age of 2.7 Ma (WoldeGabriel et al., 2001). The base of this flow lies 50 m above the base of the coarse-grained Puye Formation, which postdates the unconformity (WoldeGabriel et al., 2013). Thus, the maximum age of the lacuna is well constrained at PM-5, since it directly overlies the pumiceous unit, but the minimum age is not as tight. Well OT-4 lies on the upper end of the same fault ramp as PM-5. Well OT-4 has relatively similar subsurface age constraints for the Miocene-Pliocene unconformity, which directly overlies the 6.8–7.0 Ma pumiceous interval and underlies, by 50 m, a subsurface basalt dated at 2.5 Ma (WoldeGabriel et al., 2001, 2013). Well R-9 has an 8.5 Ma basalt interbedded in the Chamita Formation at a depth of 45 m below the Miocene-Pliocene unconformity. Series of basalts interbedded in the Puye Formation range from 2.5 to 2.1 Ma, and the base of this basalt package occurs 91 m above the Miocene-Pliocene unconformity. The easternmost well used in the Española Basin, OT-1, lies 600 m northwest of well R-9, and its subsurface basalts are inferred to correlate with those of R-9. At OT-1, the 8.5 Ma basalt directly underlies the Miocene-Pliocene unconformity and provides a tight maximum age constraint for this feature. However, there is an ~100 m section of strata between the unconformity and the next dated units (2.5–2.1 Ma basalts interbedded in the Puye Formation). There may be a west-down fault between the wells on the south-dipping ramp (PM-5 and OT-4) and the R-9 and OT-1 wells to the east (David Broxton, 2013, personal commun.). This fault may explain why there is no preserved pumiceous unit in wells R-9 and OT-1 and why the 8.5 Ma basalts are in close proximity to the unconformity (within 0–45 m).

Stratigraphic thicknesses were measured from published stratigraphic sections derived from well logs and measured sections (see Tables 3–13 for references). Well GR-4 has eight layers with age control; the Albuquerque CDRP-CL

TABLE 11. STRATIGRAPHIC SECTION ZF&AO, ALBUQUERQUE BASIN

Lithologic unit	Top (km)	Base (km)	Age top (Ma)	Age base (Ma)	ρ	*C*	φ_0	Data source
Age of Ceja Formation above basal contact up to Nomlaki Tuff	0.0	0.031	3.28	3.9*	2170	0.27	0.33	a, b, c
Inferred lacuna age range of Miocene-Pliocene unconformity	0.031	0.031	3.9*	6.0	0	0	0	a
Arroyo Ojito Formation between Peralta Tuff and upper contact	0.031	0.131	6.0	6.85	2170	0.29	0.33	a, b, c
Arroyo Ojito Formation between basal contact and Peralta Tuff	0.131	0.469	6.85	10.0	2170	0.29	0.33	a, b, c
Cerro Conejo Formation	0.469	0.789	10.0	15.0	2170	0.29	0.33	a, b, c

Note: ρ—density (kg/m³), *C*—porosity-depth coefficient, φ_0—porosity at surface. Data sources: a—Connell et al. (2013), b—Drenth et al. (2013), c—Rowan et al. (2003).
*Indicates age that is extrapolated from stratal accumulation rates calculated between Namlaki Tuff and poorly constrained base of the underlying normal-polarity interval (N1 of fig. 9 from Connell et al., 2013); note that the upper interval is on the immediate hanging wall of a fault, and stratal accumulation rates likely reflect movement along that fault.

TABLE 12. STRATIGRAPHIC SECTION CDRP-CL, ALBUQUERQUE BASIN

Lithologic unit	Top (km)	Base (km)	Age top (Ma)	Age base (Ma)	ρ	*C*	φ_0	Data source
Rio Puerco Member below Llano de Albuquerque	0.0	0.023	1.6	1.9	2170	0.2	0.21	a, b, c
Inferred lacuna age range of disconformity between Rio Puerco and Atrisco Members of Ceja Formation	0.023	0.023	1.9	2.4	0	0	0	a
Top of Atrisco Member, Ceja Formation to base of paleomagnetic reversal (assumes reversal is Kaena)	0.023	0.042	2.4	3.1	2170	0.36	0.35	a, b, c
Atrisco Member, Ceja Formation between base of paleomagnetic reversal and basal contact (assumes reversal is Kaena and basal strata postdate the Mammoth reversal)	0.042	0.055	3.1	3.2	2170	0.36	0.35	a, b, c

Note: ρ—density (kg/m^3), *C*—porosity-depth coefficient, φ_0—porosity at surface. Data sources: a—Connell et al. (2013), b—Drenth et al. (2013), c—Rowan et al. (2003).

and the ZF and AO stratigraphic sections in the Albuquerque Basin have the fewest (five age-controlled layers). The thickness of sections used ranges from 55 m (CDRP-CL) to 1.45 km (Rio Salado). Subsidence analysis results are grouped by basin in Figure 4 with ~15 m.y. *x* axes for ease of comparison.

Results: Tectonic Subsidence Curves of the Rio Grande Rift

Most tectonic subsidence curves (Fig. 4) show rapid tectonic subsidence (~25–65 mm/k.y.) in middle-late Miocene time, followed by an unconformity (horizontal segments), and renewed tectonic subsidence until ca. 3–0.5 Ma. The early ~25–65 mm/k.y. subsidence rates are similar to the prerupture phases of rifted continental margins (Xie and Heller, 2009). Postunconformity tectonic subsidence rates are similar to or less than the pre-unconformity rates (Fig. 4). The duration of the unconformity is poorly constrained in the La Jencia and Albuquerque Basins (Rio Salado, CDRP3, CDRP-CL sections), hampering comparison of pre- and postunconformity rates. We do not have tectonic subsidence rates for the later Quaternary, but paleoseismic studies indicate that several rift faults remain active (Fig. 2). In the following, we discuss the geologic context for wells in each rift basin, because the interpretation of tectonic subsidence rates is informed by the locations of the wells and stratigraphic sections relative to faults (i.e., hanging wall, footwall) and geologic features such as basalt flows.

Both wells in the San Luis Basin lie within the structurally deepest area of the basin (Grauch et al., 2017) and show similar subsidence histories (Fig. 4). It is not known if the Miocene-Pliocene unconformity is present in these wells. The Airport well (Taos Airport well of Grauch et al., 2017) is located in the Los Cordovas fault zone on the west side of the structural low, and the K3 well lies within the western (inner) side of a 6-km-wide fault system bounding the southeastern side of this structural low (Fig. 3; Grauch et al., 2017). Both wells show relatively rapid tectonic subsidence before ca. 9 Ma, decreasing tectonic subsidence from ca. 9 to 4.7 Ma, a brief rapid subsidence period between 4.7 and 3.6 Ma, and then very slow subsidence. Tectonic subsidence rates after 3.6 Ma in the K3 well are similar to those between 14 and 9 Ma in the Airport well, and the post–5 Ma record is too short for meaningful comparison.

Española Basin wells (PM-5, OT-1, OT-4, GR-4, and R-9) all are in the proximal hanging wall of the Pajarito fault (<15 km from the fault), which is the east-down master fault of the Española Basin half graben (Golombek, 1983; Koning

TABLE 13. STRATIGRAPHIC DATA, RIO SALADO BETWEEN LEMITAR MOUNTAINS AND SIERRA LADRONES

Lithologic unit	Top (km)	Base (km)	Age top (Ma)	Age base (Ma)	ρ	*C*	φ_0	Data source
Sierra Ladrones Formation	0.0	0.36	3.23*	5.0†	2170	0.25	0.29	b, c, e, m
Approximate age range of lacuna	0.36	0.36	5.0†	7.0†	0	0	0	b, c, e
Upper Popotosa Formation	0.360	2.55	7.0†	14.5§	2170	0.22	0.29	b, c, e
Upper Popotosa Formation	2.55	3.36	14.5§	15.4#	2350	0.22	0.29	b, c, e

Note: ρ—density (kg/m^3), *C*—porosity-depth coefficient, φ_0—porosity at surface. Data sources: b—Drenth et al. (2013), c—Rowan et al. (2003), e—Cather and Read (2003), m—Lueth et al. (2016). Stratigraphic thicknesses are from cross-section A-A' of Cather and Read (2003).

*3.23 ± 0.03 Ma (from cryptomelane) is the age of Riley Travertine, which caps the Sierra Ladrones Formation along Rio Salado (Lueth et al., 2016).

†Lacuna between the Sierra Ladrones Formation and Popotosa Formation is inferred to be 7–5 Ma based on regional stratigraphy (unit Tbsh of Chamberlin and Osburn, 2006; unit Tas of Chamberlin et al., 2001).

§Ash bed interbedded in Upper Popotosa Formation.

#Silver Creek andesite, dated using ^{40}Ar/^{39}Ar at 15.33 ± 0.07 Ma and 15.49 ± 0.20 Ma (R.M. Chamberlin and W.C. McIntosh, 2003, written commun., cited *in* Cather and Read, 2003).

et al., 2013). Well GR-4 lies on a structural high between two relatively deep intrabasin half grabens (the Los Alamos graben to the south and the Santa Clara graben to the north); wells PM-5 and OT-4 are located on a south-dipping structural ramp on the north side of the Los Alamos graben (Cole et al., 2009; Koning et al., 2013).

Most of the Española Basin wells (i.e., R-9, OT-1, OT-4, and GR-4) show slower tectonic subsidence rates after the lacuna than before. Well PM-5 shows slowing subsidence from ca. 7 to 3 Ma but no unconformity (flat segment), likely due to it being in a structurally deeper position in the Los Alamos graben alongside the Pajarito fault zone and to activity on the Pajarito fault itself. This is consistent with increasing Quaternary slip rates on the Pajarito fault (Koning et al., 2013). Well GR-4 is located on a structural high between two deep subbasins of the larger Española Basin (Koning et al., 2013), which may explain the relatively long duration of its lacuna.

In contrast to San Luis and Española Basins sites, located near basin-bounding faults, Albuquerque Basin sites are on or near the basin's western faulted flexural hinge (Fig. 3). These three measured sections (from Connell et al., 2013) are challenging to compare because they span different times. The duration of the Miocene-Pliocene unconformity at Albuquerque Basin sites is constrained by extrapolation of stratal accumulation rates from above and below, with age control from magnetostratigraphy and ages of lava flows, tephra, and clasts (Connell et al., 2013). Extrapolation of stratal accumulation rates suggests the lacuna here spans ca. 6 Ma to 3 Ma (site CDRP3) or 6–4 Ma (site ZFAO; Fig. 4; Tables 10–11); note that the lacuna here is not as tightly constrained as in the Española Basin. The postunconformity part of the section at site ZFAO was measured on the immediate hanging wall of a fault and so likely reflects local activity of that fault.

The Rio Salado section is in a west-tilted fault block on the northeastern side of the La Jencia Basin. Age constraints for the Rio Salado site (Chamberlin, 2004) are from dated rhyolitic ash beds, basaltic andesite layers, and a travertine (Chamberlin, 2004; Cather and Read, 2003; Lueth et al., 2016). Tectonic subsidence there (Fig. 4D) was rapid before ca. 7 Ma. An unconformity is inferred to span ca. 7–5 Ma (very poor age control), with subsidence rate afterward being slightly less than before. Early extension was on rotational domino faults that were eventually abandoned and crosscut by younger, mostly steeper faults (Chamberlin, 1983; Cather et al., 1994; Chamberlin et al., 2016). Uplift of the younger faults' footwalls may have decreased the tectonic subsidence rate at this site.

We propose that the following features are related: the widespread late Miocene–early Pliocene unconformity in the Rio Grande rift, the presence of a similar-aged unconformity in the Ocate volcanic field east of the rift, synchronous tilting of the western Great Plains, and either a slowing down or zero tectonic subsidence rate in studied locations in the late Miocene to early Pliocene. These observations span a spatial scale of ~400 by 600 km. Previous studies have mainly focused on a single or a few of these observations, and thus proposed mechanisms for their occurrence were often more local in scale or cannot address all observations (Rio Grande rift opening–related rock uplift—Steven et al., 1997; isostatic rock uplift—Leonard et al., 2002; southern Rocky Mountains uplift—McMillan et al., 2006; crustal heating—Eaton, 2008; northward propagation of the rift—Duller et al., 2012; Jemez Lineament–related magmatism and buoyancy—Nereson et al., 2013; Repasch et al., 2017; climate effects—Duller et al., 2012; Nereson et al., 2013).

Considering all observations, we suggest that a larger-scale epeirogenic event related to mantle buoyancy may provide an explanation of the mechanism involved. The role of mantle buoyancy in elevation compensation can be established with geoid-topography analyses, as described in the next section.

TOPOGRAPHIC COMPENSATION OF THE RIO GRANDE RIFT

If the unconformity, slowing of tectonic subsidence, and tilting of the western Great Plains were influenced by mantle upwelling, there may still be relic dynamic uplift related to this mantle upwelling today, since upper-mantle convection time scales below the rift are millions to tens of millions of years (van Wijk et al., 2010; Sleep, 2011). Here, we combine topographic information with geoid information to provide insight into the degree of isostatic support of the entire Rio Grande rift region. The average elevation of the Rio Grande rift changes markedly from north to south, decreasing from ~2300 m in the northern San Luis Basin to ~1200 m at the Texas–New Mexico border (Figs. 1 and 6). There is a corresponding decrease in lithospheric geoid anomaly (calculated using the method described in Coblentz at al., 2011; see following discussion) from ~10 m to 3 m (Fig. 6). We used this topographic/geoid analysis to evaluate (1) the degree to which dynamic uplift is supporting the elevation of the Rio Grande rift, and (2) the observed physiographic change along the rift axis (north of ~34°N, the rift is characterized by narrow basins with raised margins; south of 34°N, the character of the rift changes abruptly to one of parallel grabens or half grabens similar to the structure of the Basin and Range Province).

Topographic Power Spectrum of the Rio Grande Rift

We first evaluated the topographic power spectrum of the rift. This yielded information about the frequency content of the topographic signal. Here, we investigated the radial spectral power within three wavelength bands (Fig. 6) using a two-dimensional fast Fourier transform for the topography shown in Figure 6B within a moving window. Specifics of the three bands are:

(A) short wavelengths, $\lambda < 30$ km, window size = 0.5° × 0.5° (Nyquist wavelength of ~60 km),
(B) medium wavelengths, 50 km < λ < 150 km, window size = 2.0° × 2.0° (Nyquist wavelength ~240 km), and
(C) long wavelengths, $\lambda > 200$ km, window size = 4° × 4° (Nyquist wavelength ~475 km).

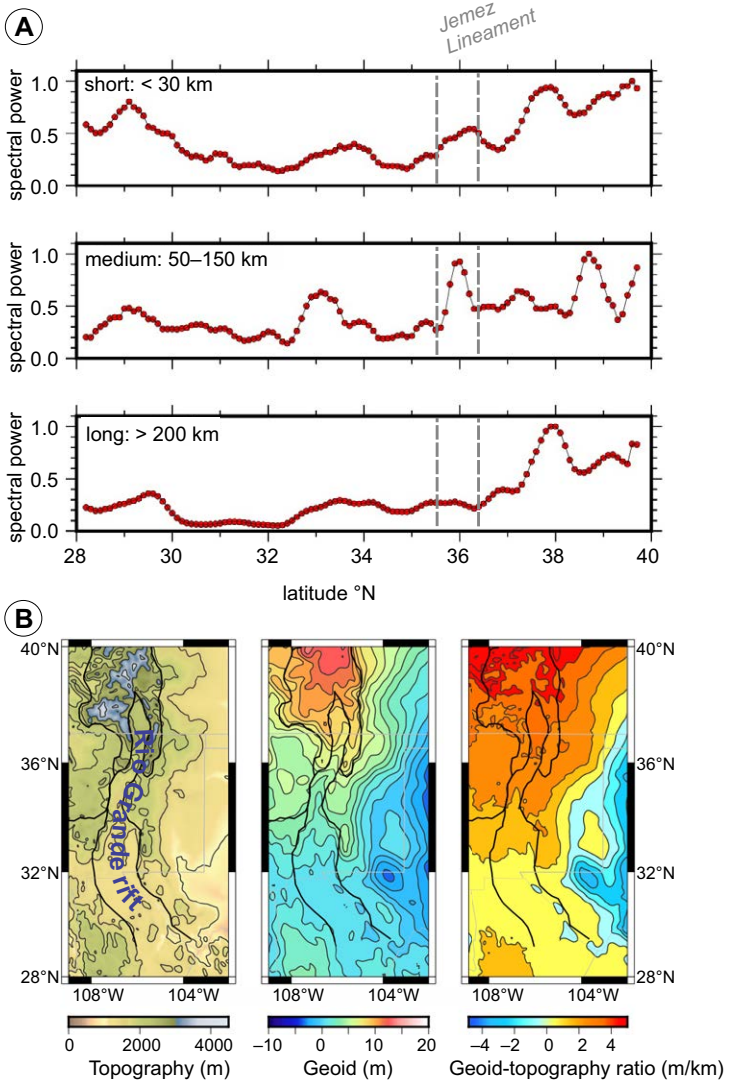

Figure 6. (A) Topographic spectral power along the Rio Grande rift for three wavelength bands, plotted as a function of latitude. Gray dashed lines outline the location of the Jemez Lineament. Upper panel: wavelength < 30 km, window size = 0.5° × 0.5°; middle panel: wavelength 50–150 km, window size = 2.0° × 2.0°; lower panel wavelength >200 km, window size = 4° × 4°. (B) Topography, geoid, and geoid-topography ratio in the Rio Grande rift region. Methods are described in the text.

The map in Figure 6B (left panel) is of the region that was used to compute the spectral power. A window with topographic information was created every 0.25° (from N to S) with a N-S width of 0.5° (for short wavelength, and larger widths for longer wavelengths, see above). After the topography was extracted, the spectral power was computed, and the power for the three bands was extracted to create one of the red points in each of the panels shown Figure 6A. This was repeated along the entire N-S region shown on the map.

Figure 6A shows the topographic spectral power for the three wavelength bands plotted parallel to the axis of the Rio Grande rift. At the shortest topographic wavelengths, the spectral power is highest in the southern rift, south of ~31°N (reflecting the dominance of Basin and Range geomorphology in the topographic signal) and north of ~37°N (reflecting the high topographic relief and roughness of the topography of the Southern Rockies in central Colorado). At medium wavelengths, spectral power is fairly uniform along the rift axis, with significant variation in the topographic power spectrum associated with the Aspen Uplift of central Colorado (~39°N; MacCarthy et al., 2014), the San Juan Mountains (~37°N to 38°N), the Jemez Lineament (centered at ~36°N), the Southern Basin and Range near 33°N, and south of the Mazatzal-Grenville suture at ~30°N. At very long wavelengths (>200 km), the power spectrum along the Rio Grande rift is dominated by the long-wavelength topographic swell of the Rocky Mountains (north of ~37°N).

Geoid-Topography Ratios of the Rio Grande Rift: Methodology

The ratio between the average elevation of the Rio Grande rift and the lithospheric geoid provides information about the compensating mechanism for the topography, and therefore the degree to which dynamic uplift from the upper mantle is supporting the topography. Geoid height anomalies for isostatically compensated regions can be directly related to the local density dipole moment, which can be used to evaluate the subsurface distribution of mass associated with various surface features (see review and discussion in Coblentz et al., 2015). Given the important role that density variations in the uppermost mantle play in rift dynamics, it is of primary interest to constrain the depth of the density distributions that control the lithospheric geoid. Because the geoid reflects the gravitational dipole moment, it is more sensitive to deeper sources than the gravity field—a consequence of the fact that the geoid anomaly observed at the surface caused by a point mass buried at depth d decreases in amplitude as $1/d$, whereas the gravity anomaly of the same point mass decays as $1/d^2$. This makes the study of geoid anomalies useful for evaluating the depth of isostatic compensation.

An evaluation of the geoid signal associated with density variations in the upper mantle requires the removal of the long-wavelength geoid signals arising from sources in the lower mantle. Here, we generated a "lithospheric geoid" by filtering the spherical harmonic terms used in the harmonic expansion of the geoid to extract the geoid signal from the uppermost mantle density variations (method described in detail in Coblentz et al., 2011). The linear

relationship between the geoid and topography can be used in a variety of ways for geodynamic applications. At wavelengths greater than the flexural wavelength (i.e., features that are isostatically compensated), geoid anomalies caused by long-wavelength continental topography are proportional to the elevation multiplied by the mean depth of compensation (Coblentz et al., 2011). Consequently, for a particular elevation, the greater the average depth of the isostatic "root," the larger is the geoid anomaly. In this case, the geoid-to-topography ratio (GTR) can be used to estimate the depth of compensation of crustal plateaus (Haxby and Turcotte, 1978). In the spatial domain, the GTR can be calculated by simply dividing the average geoid by the average elevation (usually in km; Chase et al., 2002), shown in Figure 6, or by plotting the geoid height against topography and calculating the slope of the fit to the data in a traditional least squares method (Sandwell and MacKenzie, 1989; Sandwell and Renkin, 1988).

Under the assumption that topography is locally compensated at wavelengths greater than the flexural wavelength (~400 km), the geoid height is proportional to the dipole density moment (Ockendon and Turcotte, 1977). The geoid-to-topography ratio (GTR) depends on the average depth of compensation (Haxby and Turcotte, 1978). Topographic features with GTR greater than ~6 m/km are compensated beneath the lithosphere and therefore must have a significant component of dynamic support by convective stresses (McKenzie et al., 1980). In contrast, low GTR vales (in the range of 0–2 m/km) are associated with shallow (<50 km) Airy or Pratt compensation (Angevine and Turcotte, 1983). In the middle range, for GTR values between 2 and 6 m/km, topography is compensated at depths between 50 and 80 km, likely related to lithosphere thinning (Crough, 1978).

Geoid-Topography Ratios of the Rio Grande Rift: Results

The GTR gradually increases northward north of 32°N, i.e., southern New Mexico. The GTR (Fig. 6B) is around or below 2 m/km south of the Socorro accommodation zone (~34°N), which means that the southern Rio Grande rift is at present isostatically compensated by shallow Airy isostasy. The GTR steadily increases to 40°N, where the value of 5 m/km is close to the dynamic support threshold. The large GTR in the northern part of the rift (north of 35°N in the Albuquerque Basin) supports an interpretation that the northern Rio Grande rift at present still has a component of mantle-driven dynamic uplift.

DISCUSSION

What Caused the Miocene-Pliocene Unconformity in the Rio Grande Rift Region and Tilting of the Western Great Plains?

Most of the tectonic subsidence curves (Fig. 4) are consistent with a phase of slow-down or absence of tectonic subsidence in the late Miocene–early Pliocene. Such patterns in tectonic subsidence curves indicate a smaller or absent accommodation space and can typically be explained by a slow-down of rift opening, or a process such as dynamic uplift. Because our geoid analysis indicates that there is at present a component of dynamic compensation of topography in the northern rift region, and there are geophysical indications for dynamic surface uplift in the rift region (Moucha et al., 2008), we focus here on dynamic uplift as a mechanism for a slow-down in tectonic subsidence, the Miocene-Pliocene unconformity, and eastward tilting of the western Great Plains.

Mantle-driven dynamic uplift below the Rio Grande rift region is the result of a combination of factors: foundering and fragmentation of the Farallon slab and related convection patterns, opening of the Rio Grande rift, and the relative motion between North America and the underlying asthenosphere (Moucha et al., 2008; van Wijk et al., 2008, 2010; Ricketts et al., 2015; Ricketts and Karlstrom, 2016). Moucha et al. (2008) calculated that as a result of this mantle flow, dynamic uplift occurred in the Rio Grande rift region in the last ~10 m.y. The total amplitude of dynamic topography is difficult to estimate, but may be hundreds of meters (Moucha et al., 2008). In their study, the "bull's-eye" of the dynamically uplifted region passed over the central-northern Rio Grande rift and caused most dynamic uplift there. In the southern Rio Grande rift, the amplitude of dynamic topography is expected to have been smaller (Moucha et al., 2008). This could explain the more widespread nature of the Miocene-Pliocene unconformity in the Española Basin region.

Our tectonic subsidence curves (Fig. 4) suggest that prior to the unconformity, tectonic subsidence rates varied (in the locations that we analyzed) between ~25 and 65 m/m.y.; present-day dynamic uplift calculated by Moucha et al. (2008) ranges from ~15 m/m.y. in the southern rift to ~30 m/m.y. in the northern rift, and the uplift rate may have been higher in the past when the "bull's-eye" of dynamic uplift passed below the rift (Moucha et al., 2008). In places, the dynamic uplift rate thus may have exceeded the tectonic subsidence rate, resulting in a local diminishment of accommodation space within the rift zone that may have promoted erosion. Because unconformities form as a result of the interplay among uplift, tectonic subsidence, and sediment discharge, and because the tectonic subsidence varies from location to location in the rift (Fig. 4), we do not expect that the unconformity was synchronous in the Rio Grande rift, nor that it formed everywhere. The amount of material that was eroded cannot be determined; assuming an erosion rate of 5 m/m.y. yields a total of 25 m of erosion over the time span of a 5 m.y. lacuna. Because North America moves southwestward with respect to the underlying mantle, and upper-mantle convection patterns change over time scales of millions to tens of millions of years, the dynamic uplift is a transient phenomenon. In the southern rift, it no longer compensates topography, in agreement with predictions of our geoid-topography analysis.

Formation of the Miocene-Pliocene unconformity within the rift has likely resulted from an interplay of processes. When accommodation space reduced because of dynamic uplift, the efficacy of other mechanisms was enhanced. Within the rift, these mostly involved stratal onlap and offlap relative to basin margins. As suggested by Cather et al. (1994), higher tectonic subsidence rates prior to the unconformity may have induced offlap (from basin margins), while

lower rates after the unconformity produced stratal onlap. Climate changes involving progressive aridification in the late Miocene (MacFadden, 1992; Webb and Opdyke, 1995), followed by the 7–5 Ma intensification of the North American monsoon (Chapin, 2008), could have dramatically changed sediment flux into rift basins, producing offlap (and associated unconformity development) and then onlap of active sedimentation on basin margins (see Connell et al., 2013). Changes in stream competency (Connell et al., 2013) and sediment fluxes related to 7–5 Ma climate changes could also have affected erosion of the regional landscape.

Our findings are consistent with previous work suggesting that the high elevation of the San Juan Mountains (Southern Rockies) just west of the northern Rio Grande rift results from mantle-driven uplift (Karlstrom et al., 2012; Hansen et al., 2013), and that flexural deformation and density anomalies may have played a secondary role (Roy et al., 2004; Hansen et al., 2013). Our study also supports conclusions by Nereson et al. (2013) and Repasch et al. (2017) that dynamic topography played a large role in river incision in the Ocate volcanic field and northern Rio Grande rift; here, we suggest that the cause of the dynamic uplift is the E-W passage of the thermally driven vertical flow below the Colorado Plateau and Rio Grande rift documented by Moucha et al. (2008). This effect may have been enhanced locally by magmatic buoyancy of the Jemez Lineament (Nereson et al., 2013; Repasch et al., 2017), resulting in the more prominent and widespread unconformity observed in the Española Basin. We find that this thermally driven, vertical mantle flow may also have caused uplift of the western part of the Great Plains, tilting the Ogallala Formation eastward.

Insight into Rift Opening from Tectonic Subsidence Curves

The tectonic subsidence curves (Fig. 4) suggest that the tectonic subsidence rate either remained similar or decreased after the lacuna. Field studies show a generally low tilt of Pliocene–Pleistocene strata, which was interpreted previously (Cather et al., 1994) as a tectonic slow-down in the northern Rio Grande rift basins after 7–5 Ma. Although the Airport well in the southern San Luis Basin shows a general post–7–5 Ma slow-down directly following the unconformity, the tectonic subsidence rate actually increases for a short period of time (Fig. 4). The short post–5 Ma stratigraphic record of the K3 well makes post- versus pre-unconformity rate comparisons difficult. Three of the studied wells in the Española Basin allow for a post–5 Ma slow-down (OT-1, OT-4, GR-4); the other two (R-9 and PM-5) suggest a continuance of rates. In several locations, there is insufficient record for comparison (Albuquerque Basin), or shifting of fault strain may be involved (Rio Salado section). None of the subsidence curves yielded evidence for increasing rates of tectonic subsidence since the Miocene-Pliocene unconformity, possibly due to the ongoing effects of dynamic uplift.

Our subsidence curves reflect only the past ~15 m.y., but thermochronology data compiled by Ricketts et al. (2015) indicate relatively synchronous rapid cooling (uplift) of rift flanks bounded by master faults along the entire north-south extent of the Rio Grande rift at ca. 20 Ma, which has been interpreted as relatively simultaneous rift opening. Earlier studies (Baldridge et al., 1994; Ingersoll, 2001) described rift histories with possible periods of faster or slower rift opening, and migration of deformation when some of the early rift faults became inactive. These studies seem to agree that rapid opening was occurring by 21 Ma, followed by a phase of slower rift opening (likely under way by 10 Ma, when some of the early rift faults had become inactive), which was interpreted by Ebinger et al. (2013) as related to strain repartitioning due a rotation in the far-field stresses in the southwestern United States. Because the pre–15 Ma period is missing from our tectonic subsidence curves, it is not possible to say whether they support these earlier studies.

Net horizontal Rio Grande rift extension can be inferred from seismic studies (Kluth and Schaftenaar, 1994; Russell and Snelson, 1994). As reviewed earlier herein, net extension in the San Luis Basin is 4.5–6.5 km and started between 30 and 26 Ma, yielding long-term average rates of 0.25–0.35 mm/yr. Net extension in the Albuquerque Basin is ~10 km in the north and ~17 km in the south, and extension there probably began between ca. 30 and 32 Ma, yielding average horizontal extension rates of 0.3–0.6 mm/yr. If rapid extension began at ca. 20 Ma and lasted until ca. 5 Ma, with very little subsequent extension, then the range of average horizontal extension rates is ~0.3–0.4 mm/yr (San Luis Basin) and ~0.7–1.1 mm/yr (Albuquerque Basin). We suggest that high Quaternary opening rates in the west-central Albuquerque Basin (Ricketts et al., 2014) represent a locally intense rifting event of short duration, as part of the opening cycle of continental rift zones (Ebinger et al., 2013), in which places and periods of rapid opening alternate with quiet phases. As mentioned already, at present, the strain across the rift is ~1 mm/yr, as measured in baselines of ~1000 km length that extend from the Great Plains to the Colorado Plateau (e.g., Murray et al., 2015). In conclusion, Rio Grande rift opening is continuing at present, but there are no indications that rift opening has accelerated since the lacuna.

Role of Mantle Upwelling in Rift Opening

Numerical modeling work (Burov and Guillou-Frottier, 2005) predicts that active, dynamic surface uplift, such as that caused by thermal plumes or focused mantle upwelling, creates tensional forces in the lithosphere that are large enough to drive lithosphere extension and cause rifting or, in concert with lithosphere thinning, focus and accelerate rifting (Burov and Gerya, 2014; Koptev et al., 2015). Rift focusing and accelerated rift opening are predicted in studies where the lithosphere is stretched by plate-tectonic forces above focused mantle upwelling (Burov and Gerya, 2014; Koptev et al., 2015). Examples of rift basins that have been formed or were strongly affected by this process are found in the eastern and western branches of the central East African Rift (Ebinger and Sleep, 1998; Koptev et al., 2015). In the East African Rift, focused mantle upwelling occurred prior to or at the onset of rifting, and the rift ba-

sins thus formed after focused mantle upwelling affected the region. The Rio Grande rift provides a unique opportunity to test how focused mantle upwelling affects rift opening because it experienced focused thermal upwelling that caused the lacuna (described as a weak mantle plume by Moucha et al., 2008) during the later rift stage, so that rift opening before and after the arrival of the mantle driving force can be compared. Further, rift opening, tectonic subsidence, and stratigraphy are all well documented before and after the lacuna.

Our analyses of tectonic subsidence and a literature review of opening rates and rift-stratigraphy suggest that there is no evidence for syn- or post-lacuna accelerated rift opening or tectonic subsidence in the Rio Grande rift. Rio Grande rift opening continued after establishment of the focused mantle upwelling but did not accelerate; field observations of little-deformed strata overlying the unconformity (e.g., Bryan and McCann, 1938; Wright, 1946; Spiegel and Baldwin, 1963; Stearns, 1979; Seager et al., 1984; Connell et al., 2013; Cather et al., 1994) suggest that rift opening may, in fact, have slowed down after the lacuna.

What may explain this discrepancy between Rio Grande rift observations and numerical predictions? One explanation is that the focused upwelling below the northern Rio Grande rift may be weaker than upwelling in numerical studies, so that its effect is smaller. Although Wilson et al. (2005) imaged up to ~6% lower seismic shear wave velocities at asthenospheric depths below the Rio Grande rift, seismic shear wave anomalies at transition zone depths of the focused upwelling zone below the rift are generally less than ~1% (Moucha et al., 2008), corresponding to a <100 K thermal anomaly (Cammarano et al., 2003). In Koptev et al. (2015), a 200-km-radius, 300 K thermal anomaly was emplaced at the base of the transition zone to induce the focused vertical mantle flow pattern; this created a stronger upward flow. We further note that the mantle lithosphere of the Rio Grande rift was already thinned before the focused mantle upwelling affected the region (van Wijk et al., 2008; Moucha et al., 2008); in numerical modeling studies (Burov and Gerya, 2014; Koptev et al., 2015), thermal erosion of the mantle lithosphere by a plume head is a major reason for focusing and intensification of rifting.

CONCLUSIONS

Our backstripping analyses of wells and stratigraphic sections with adequate age control (≤15 m.y.) show that tectonic subsidence in the Rio Grande rift occurred at rates of a few tens of meters per million years in all studied basins since 15 Ma. This rate falls within the normal range of tectonic subsidence rates for the pre-breakup phase of rifted margins. Prior to the unconformity, many kilometers of sediments accumulated in the rift basins.

The Miocene-Pliocene unconformity is present along the flanks of most rift basins from central Colorado to southern New Mexico, and in the Ocate volcanic field east of the rift, and is synchronous with eastward tilting of the western Great Plains. The exact duration of the lacuna depends on location within the rift but in general includes the time period of 7–5 Ma. The widespread occurrence of the unconformity, including its extent outside of the rift in northern New Mexico, means it cannot be due solely to changes in rift opening rate, as previously suggested. Synchronous tilting of the Ogallala Formation rules out concomitant climatic changes as a sole cause. A comparison between the mapped extent of the unconformity and geoid-topography ratios reveals that topography in the northern rift is still supported by a component of dynamic uplift, and we infer that this mantle-driven dynamic uplift in New Mexico and south-central Colorado promoted the development of the unconformity and caused eastward tilting of the Ogallala Formation in the western Great Plains. The focused vertical mantle flow results from an interplay between Rio Grande rift opening and Farallon slab descent and fragmentation. Unlike the East African Rift zone, no evidence is found in the Rio Grande rift for focused thermal mantle upwelling playing an important role in rift focusing and intensification.

ACKNOWLEDGMENTS

We thank the reviewers (Karl Karlstrom, Giacomo Corti, and an anonymous reviewer) and the editor for very constructive comments. We would like to thank Kent Condie, Ahmad Malekpour, Rediet Abera, Jeff Dobbins, Steve Cather, and Richard Chamberlin for fruitful discussions. Andy Jochems provided assistance with Table 1. Giday WoldeGabriel and David Broxton of Los Alamos National Laboratory were extremely helpful in sharing and discussing age control of subsurface data in the western Española Basin. Axen and van Wijk were supported by National Science Foundation grant EAR-1348076.

REFERENCES CITED

Aby, S., 2008, Preliminary Geologic Map of the Servilleta Plaza 7.5-Minute Quadrangle Map, Taos County, New Mexico: New Mexico Bureau of Geology and Mineral Resources Open-File Geologic Map OF-GM 182, scale 1:24,000.

Angevine, C.L., and Turcotte, D.L., 1983, Correlation of geoid and depth anomalies over the Agulhas Plateau: Tectonophysics, v. 100, p. 43–52, https://doi.org/10.1016/0040-1951(83)90177-4.

Appelt, R.M., 1998, $^{40}Ar/^{39}Ar$ Geochronology and Volcanic Evolution of the Taos Plateau Volcanic Field, Northern New Mexico and Southern Colorado [M.S. thesis]: Socorro, New Mexico, New Mexico Institute of Mining and Technology, 58 p.

Baldridge, W.S., Ferguson, J.F., Braile, L.W., Wang, B., Eckhardt, K., Evans, D., Schultz, C., Gilpin, B., Jiracek, G.R., and Biehler, S., 1994, The western margin of the Rio Grande rift in northern New Mexico: An aborted boundary?: Geological Society of America Bulletin, v. 106, p. 1538–1551, https://doi.org/10.1130/0016-7606(1994)106<1538:TWMOTR>2.3.CO;2.

Baldridge, W.S., Keller, G.R., Haak, V., Wendlandt, E., Jiracek, G.R., and Olsen, K.H., 1995, The Rio Grande rift, *in* Olsen, K.H., ed., Continental Rifts: Evolution, Structure, Tectonics: Amsterdam, Netherlands, Elsevier, Developments in Geotectonics 25, p. 233–275.

Bauer, P.W., Kelson, K.I., and Aby, S.B., 2005, Geologic Map of the Peñasco Quadrangle, Taos County, New Mexico: New Mexico Bureau of Geology and Mineral Resources Open-File Digital Geologic Map OF-GM 062, scale 1:24,000.

Beutel, E., van Wijk, J., Ebinger, C., Keir, D., and Agostini, A., 2010, Formation and stability of magmatic segments in the Main Ethiopian and Afar Rifts: Earth and Planetary Science Letters, v. 293, p. 225–235, https://doi.org/10.1016/j.epsl.2010.02.006.

Bialas, R.W., Buck, W.R., and Qin, R., 2010, How much magma is required to rift a continent?: Earth and Planetary Science Letters, v. 292, p. 68–78, https://doi.org/10.1016/j.epsl.2010.01.021.

Bird, P., 1984, Laramide crustal thickening event in the Rocky Mountain foreland and Great Plains: Tectonics, v. 3, p. 741–758, https://doi.org/10.1029/TC003i007p00741.

Bond, G.C., and Kominz, M.A., 1984, Construction of tectonic subsidence curves for the early Paleozoic miogeocline, southern Canadian Rocky Mountains: Implications for subsidence mechanisms, age of breakup, and crustal thinning: Geological Society of America Bulletin, v. 95, p. 155–173, https://doi.org/10.1130/0016-7606(1984)95<155:COTSCF>2.0.CO;2.

Brister, B.S., and Gries, R.R., 1994, Tertiary stratigraphy and tectonic development of the Alamosa basin (northern San Luis Basin), Rio Grande rift, south-central Colorado, *in* Keller, G.R., and Cather, S.M., eds., Basins of the Rio Grande Rift: Structure, Stratigraphy, and Tectonic Setting: Geological Society of America Special Paper 291, p. 39–58, https://doi.org/10.1130/SPE291-p39.

Broxton, D., Gilkeson, R., Longmire, P., Marin, J., Warren, R., Vaniman, D., Crowder, A., Newman, B., Lowry, B., Rogers, D., Stone, W., McLin, S., WoldeGabriel, G., Daymon, D., and Wycoff, D., 2001, Characterization Well R-9 Completion Report: Los Alamos National Laboratory Report LA-13742-MS, 85 p.

Broxton, D.E., WoldeGabriel, G., Vaniman, D., and Koning, D.J., 2012, Mid–upper Miocene sedimentary strata in the western Española Basin, New Mexico: Geological Society of America Abstracts with Programs, v. 44, no. 6, p. 78.

Brune, S., Heine, C., Pérez-Gussinyé, M., and Sobolev, S.V., 2014, Rift migration explains continental margin asymmetry and crustal hyper-extension: Nature Communications, v. 5, 4014, https://doi.org/10.1038/ncomms5014.

Bryan, K., 1938, Geology and Ground-Water Conditions of the Rio Grande Depression in Colorado and New Mexico, *in* U.S. National Resources Planning Board, The Rio Grande Joint Investigation in the Upper Rio Grande Basin: Washington, D.C., U.S. Government Printing Office, v. 1, part 2, p. 196–225.

Bryan, K., and McCann, F.T., 1938, The Ceja del Rio Puerco: A border feature of the Basin and Range Province in New Mexico: Part II. Geomorphology: The Journal of Geology, v. 46, p. 1–16, https://doi.org/10.1086/624618.

Burov, E., and Gerya, T., 2014, Asymmetric three-dimensional topography over mantle plumes: Nature, v. 513, no. 7516, p. 85–89, https://doi.org/10.1038/nature13703.

Burov, E., and Guillou-Frottier, L., 2005, The plume head–continental lithosphere interaction using a tectonically realistic formulation for the lithosphere: Geophysical Journal International, v. 161, p. 469–490, https://doi.org/10.1111/j.1365-246X.2005.02588.x.

Burov, E., and Poliakov, A., 2001, Erosion and rheology controls on synrift and postrift evolution: Verifying old and new ideas using a fully coupled numerical model: Journal of Geophysical Research, v. 106, no. B8, p. 16,461–16,481, https://doi.org/10.1029/2001JB000433.

Cammarano, F., Goes, S., Vacher, P., and Giardini, D., 2003, Inferring upper-mantle temperatures from seismic velocities: Physics of the Earth and Planetary Interiors, v. 138, p. 197–222, https://doi.org/10.1016/S0031-9201(03)00156-0.

Cather, S.M., 1990, Stress and volcanism in the northern Mogollon-Datil volcanic field, New Mexico: Effects of the post-Laramide tectonic transition: Geological Society of America Bulletin, v. 102, p. 1447–1458, https://doi.org/10.1130/0016-7606(1990)102<1447:SAVITN>2.3.CO;2.

Cather, S.M., and Read, A.S., 2003, Geologic Map of the Silver Creek 7.5-Minute Quadrangle: New Mexico Bureau of Geology and Mineral Resources Open-File Geologic Map 75, scale 1:24,000.

Cather, S.M., Chamberlin, R.M., Chapin, C.E., and McIntosh, W.C., 1994, Stratigraphic consequences of episodic extension in the Lemitar Mountains, central Rio Grande rift, *in* Keller, G.R., and Cather, S.M., eds., Basins of the Rio Grande Rift: Structure, Stratigraphy, and Tectonic Setting: Geological Society of America Special Paper 291, p. 157–170, https://doi.org/10.1130/SPE291-p157.

Cather, S.M., Colpitts, R.B., and Hook, S.C., 2004, Geologic Map of the Mesa del Yeso Quadrangle, Socorro County, New Mexico: New Mexico Bureau of Geology and Mineral Resources Open-File Geologic Map OF-GM 92, scale 1:24,000.

Cather, S.M., Chapin, C.E., and Kelley, S.A., 2012, Diachronous episodes of Cenozoic erosion in southwestern North America and their relationship to surface uplift, paleoclimate, paleodrainage, and paleoaltimetry: Geosphere, v. 8, p. 1177–1206, https://doi.org/10.1130/GES00801.1.

Chamberlin, R.M., 1983, Cenozoic domino-style crustal extension in the Lemitar Mountains, New Mexico: A summary, *in* Chaplin, C.E., ed., Socorro Region II, 1983: New Mexico Geological Society 34th Field Conference Guidebook: Socorro, New Mexico, New Mexico Geological Society, p. 11–118.

Chamberlin, R.M., 2004, Geologic Map of the San Lorenzo Spring 7.5-Minute Quadrangle: New Mexico Bureau of Geology and Mineral Resources Open-File Geologic Map 86, scale 1:24,000.

Chamberlin, R.M., and Osburn, G.R., 2006, Preliminary Geologic Map of the Water Canyon Quadrangle, Socorro County, New Mexico: New Mexico Bureau of Geology and Mineral Resources Open-File Geologic Map 118, scale 1:24,000.

Chamberlin, R.M., Pazzaglia, F.J., Wegmann, K.W., and Smith, G.A., 1999, Geologic Map of the Loma Creston Quadrangle, Sandoval County, New Mexico: New Mexico Bureau of Geology and Mineral Resources Open-File Geologic Map OF-GM 025, scale 1:24,000.

Chamberlin, R.M., Cather, S.M., Nyman, M.W., and McLemore, V.T., 2001, Geologic Map of the Lemitar 7.5-Minute Quadrangle: New Mexico Bureau of Geology and Mineral Resources Open-File Geologic Map 38, scale 1:24,000.

Chamberlin, R.M., Love, D.W., Harrison, B.J., Lueth, V.W., Frey, B.A., Williams, S., and Connell, S.D., 2016, Sevilleta west: Pre-meeting road log from Sevilleta National Wildlife Refuge Visitor Center to San Acacia, Cerritos de las Minas, West Mesa, and San Lorenzo Spring, *in* Frey, B.A., Karlstrom, K.E., Lucas, S.G., William, S., Ziegler, K., McLemore, V., and Ulmer-Scholle, D.S., eds., The Geology of the Belen Area: New Mexico Geological Society 67th Annual Field Conference Guidebook: Socorro, New Mexico, New Mexico Geological Society, p. 37–61.

Channer, M.A., Ricketts, J.W., Zimmerer, M., Heizler, M., and Karlstrom, K.E., 2015, Surface uplift above the Jemez mantle anomaly in the past 4 Ma based on $^{40}Ar/^{39}Ar$ dated paleoprofiles of the Rio San Jose, New Mexico, USA: Geosphere, v. 11, p. 1384–1400, https://doi.org/10.1130/GES01145.1.

Chapin, C.E., 1971, The Rio Grande rift: Part 1. Modifications and additions, *in* James, H.L., ed., San Luis Basin: New Mexico Geological Society 22nd Annual Fall Field Conference Guidebook: Socorro, New Mexico, New Mexico Geological Society, p. 191–201.

Chapin, C.E., 2008, Interplay of oceanographic and paleoclimate events with tectonism during middle to late Miocene sedimentation across the southwestern USA: Geosphere, v. 4, p. 976–991, https://doi.org/10.1130/GES00171.1.

Chapin, C.E., and Cather, S.M., 1994, Tectonic setting of the axial basins of the northern and central Rio Grande rift, *in* Keller, G.R., and Cather, S.M., eds., Basins of the Rio Grande Rift: Structure, Stratigraphy, and Tectonic Setting: Geological Society of America Special Paper 291, p. 5–26, https://doi.org/10.1130/SPE291-p5.

Chase, C.G., Libarkin, J.A., and Sussman, A.J., 2002, Colorado Plateau: Geoid and means of isostatic support: International Geology Review, v. 44, p. 575–587, https://doi.org/10.2747/0020-6814.44.7.575.

Cikoski, C.T., and Koning, D.J., 2013, Geologic Map of the Huerfano Hill Quadrangle, Sierra County, New Mexico: New Mexico Bureau of Geology and Mineral Resources Open-File Geologic Map OF-GM 243, scale 1:24,000 (last modified June 2013).

Cikoski, C.T., Nelson, W.J., Koning, D.J., Elrick, S., and Lucas, S.G., 2017, Geologic Map of the Black Bluffs 7.5-Minute Quadrangle, New Mexico: New Mexico Bureau of Geology and Mineral Resources Open-File Geologic Map OF-GM 262, scale 1:24,000.

Coblentz, D., Chase, C.G., Karlstrom, K., and van Wijk, J., 2011, Topography, the geoid, and compensation mechanisms for the southern Rocky Mountains: Geochemistry Geophysics Geosystems, v. 12, Q04002, https://doi.org/10.1029/2010GC003459.

Coblentz, D., van Wijk, J., Richardson, R.M., and Sandiford, M., 2015, The upper mantle geoid: Implications for continental structure and the intraplate stress field, *in* Foulger, G.R., Lustrino, M., and King, S.D., eds., The Interdisciplinary Earth: A Volume in Honor of Don L. Anderson: Geological Society of America Special Paper 514, p. 197–214, https://doi.org/10.1130/2015.2514(13).

Cole, G., Coblentz, D., Jacobs, E., Koning, D., Broxton, D., Vaniman, D., Goff, F., WoldeGabriel, G., Simmons, A., and Heikoop, J., 2009, The 2009 Three-Dimensional, Geologic Models of the Los Alamos National Laboratory Site, Southern Española Basin, and Española Basin: Los Alamos National Laboratory Report LA-UR-09–3701, 128 p.

Connell, S.D., 2008a, Geologic Map of the Albuquerque–Rio Rancho Metropolitan Area, Bernalillo and Sandoval Counties, New Mexico: New Mexico Bureau of Geology and Mineral Resources Geologic Map GM-78, scale 1:50,000, 2 plates.

Connell, S.D., 2008b, Refinements to the stratigraphic nomenclature of the Santa Fe Group, northwestern Albuquerque Basin, New Mexico: New Mexico Geology, v. 30, no. 1, p. 14–35.

Connell, S.D., Koning, D.J., and Cather, S.M., 1999, Revisions to the stratigraphic nomenclature of the Santa Fe Group, northwestern Albuquerque Basin, New Mexico, *in* Pazzaglia, F.J., and Lucas, S.G., eds., Albuquerque Geology: New Mexico Geological Society 50th Field Conference Guidebook: Socorro, New Mexico, New Mexico Geological Society, p. 337–353.

Connell, S.D., Hawley, J.W., and Love, D.W., 2005, Late Cenozoic drainage development in the southeastern Basin and Range of New Mexico, southeasternmost Arizona, and western Texas, *in* Lucas, S.G., Morgan, G.S., and Zeigler, K.E., eds., New Mexico's Ice Ages: New Mexico Museum of Natural History and Science Bulletin 28, p. 125–150.

Connell, S.D., Smith, G.A., Geissman, J.W., and McIntosh, W.C., 2013, Climatic controls on non-marine depositional sequences in the Albuquerque Basin, Rio Grande rift, north-central New Mexico, *in* Hudson, M.R., and Grauch, V.J.S., eds., New Perspectives on Rio Grande Rift Basins: From Tectonics to Groundwater: Geological Society of America Special Paper 494, p. 383–425, https://doi.org/10.1130/2013.2494(15).

Corti, G., 2008, Control of rift obliquity on the evolution and segmentation of the Main Ethiopian Rift: Nature Geoscience, v. 1, p. 258–262, https://doi.org/10.1038/ngeo160.

Corti, G., 2012, Evolution and characteristics of continental rifting: Analog modeling-inspired view and comparison with examples from the East African Rift system: Tectonophysics, v. 522–523, p. 1–33, https://doi.org/10.1016/j.tecto.2011.06.010.

Corti, G., van Wijk, J., Bonini, M., Sokoutis, D., Cloetingh, S., Innocenti, F., and Manetti, P., 2003, Transition from continental break-up to punctiform seafloor spreading: How fast, symmetric and magmatic: Geophysical Research Letters, v. 30, 1604, https://doi.org/10.1029/2003GL017374.

Crone, A.J., and Machette, M.N., 2005, Paleoseismic activity on the Sangre de Cristo fault near San Luis, Colorado: Abstracts with Programs Geological Society of America, v. 37, no. 7, p. 558.

Crough, S.T., 1978, Thermal origin of mid-plate hot-spot swells: Geophysical Journal International, v. 55, p. 451–469, https://doi.org/10.1111/j.1365-246X.1978.tb04282.x.

Crumpler, L.S., 1982, Volcanism in the Mount Taylor region, *in* Grambling, J.A., Wells, S., and Callender, F., eds., Albuquerque Country II: New Mexico Geological Society 33rd Field Conference Guidebook: Socorro, New Mexico, New Mexico Geological Society, p. 291–298.

Dethier, D.P., 2003, Geologic Map of the Puye Wuadrangle, Los Alamos, Rio Arriba, Sandoval, and Santa Fe Counties, New Mexico: U.S. Geological Survey Miscellaneous Field Studies Map 2419, scale 1:24,000.

Drakos, P., Lazarus, J.A.Y., Riesterer, J.I.M., White, B., Banet, C., Hodgins, M., and Sandoval, J., 2004, Subsurface stratigraphy in the southern San Luis Basin, New Mexico, *in* Brister, B., Bauer, P., Read, A., and Lueth, V., eds., Geology of the Taos Region: New Mexico Geological Society 55th Field Conference Guidebook: Socorro, New Mexico, New Mexico Geological Society, p. 374–382.

Drenth, B.J., Grauch, V.J.S., and Rodriguez, B.D., 2013, Geophysical constraints on Rio Grande rift structure in the central San Luis Basin, Colorado and New Mexico, *in* Hudson, M.R., and Grauch, V.J.S., eds., New Perspectives on Rio Grande Rift Basins: From Tectonics to Groundwater: Geological Society of America Special Paper 494, p. 75–99, https://doi.org/10.1130/2013.2494(04).

Duller, R.A., Whittaker, A.C., Swinehart, J.B., Armitage, J.J., Sinclair, H.D., Bair, A., and Allen, P.A., 2012, Abrupt landscape change post–6 Ma on the central Great Plains, USA: Geology, v. 40, p. 871–874, https://doi.org/10.1130/G32919.1.

Dunbar, N., 2005, Quaternary volcanism in New Mexico, *in* Lucas, S.G., Morgan, G.S., and Zeigler, K.E., eds., New Mexico's Ice Ages: New Mexico Museum of Natural History and Science Bulletin, v. 28, p. 95–106.

Eaton, G.P., 2008, Epeirogeny in the Southern Rocky Mountains region: Evidence and origin: Geosphere, v. 4, p. 764–784, https://doi.org/10.1130/GES00149.1.

Ebinger, C.J., and Sleep, N.H., 1998, Cenozoic magmatism throughout East Africa resulting from impact of a single plume: Nature, v. 395, p. 788–791, https://doi.org/10.1038/27417.

Ebinger, C.J., van Wijk, J.W., and Keir, D., 2013, The time scales of continental rifting: Implications for global processes, *in* Bickford, M.E., ed., The Web of Geological Sciences: Advances, Impacts, and Interactions: Geological Society of America Special Paper 500, p. 371–396, https://doi.org/10.1130/2013.2500(11).

Esedo, R., van Wijk, J., Coblentz, D., and Meyer, R., 2012, Uplift prior to continental breakup: Indication for removal of mantle lithosphere?: Geosphere, v. 8, p. 1078–1085, https://doi.org/10.1130/GES00748.1.

Ferguson, J.F., Baldridge, W.S., Braile, L.W., Biehler, S., Gilpin, B., and Jiracek, G.R., 1995, Structure of the Española Basin, Rio Grande rift, New Mexico, from SAGE seismic and gravity data, *in* Bauer, P.W., Kues, B.S., Dunbar, N.W., Karlstrom, K.E., and Harrison, B., eds., Geology of the Santa Fe Region: New Mexico Geological Society 46th Annual Field Conference Guidebook: Socorro, New Mexico, New Mexico Geological Society, p. 105–110.

Foley, L.L., LaForge, R.C., and Piety, L.A., 1988, Seismotectonic Study for Elephant Butte and Caballo Dams, Rio Grande Project, New Mexico: U.S. Bureau of Reclamation Seismotectonic Report 88–9, 60 p.

Galusha, T., and Blick, J.C., 1971, Stratigraphy of the Santa Fe Group, New Mexico: American Museum of Natural History Bulletin 144, 127 p.

Gardner, J.N., Reneau, S.L., Lavine, A., Lewis, C.J., Katzman, D., McDonald, E.V., Lepper, K., Kelson, K.I., and Wilson, C., 2003, Paleoseismic Trenching in the Guaje Mountain Fault Zone, Pajarito Fault System, Rio Grande Rift, New Mexico: Los Alamos National Laboratory Report LA-14087-MS, 68 p.

Gile, L.H., 1986, Late Holocene displacement along the Organ Mountains fault in southern New Mexico—A summary: New Mexico Geology, v. 8, p. 1–4.

Gile, L.H., 1994, Soils, Geomorphology, and Multiple Displacements along the Organ Mountains Fault in Southern New Mexico: New Mexico Bureau of Mines and Mineral Resources Bulletin 133, 91 p.

Golombek, M.P., 1983, Geology, structure, and tectonics of the Pajarito fault zone in the Española Basin of the Rio Grande rift, New Mexico: Geological Society of America Bulletin, v. 94, p. 192–205, https://doi.org/10.1130/0016-7606(1983)94<192:GSATOT>2.0.CO;2.

Grauch, V.J.S., and Connell, S.D., 2013, New perspectives on the geometry of the Albuquerque Basin, Rio Grande rift, New Mexico: Insights from geophysical models of rift-fill thickness, *in* Hudson, M.R., and Grauch, V.J.S., eds., New Perspectives on Rio Grande Rift Basins: From Tectonics to Groundwater: Geological Society of America Special Paper 494, p. 427–462, https://doi.org/10.1130/2013.2494(16).

Grauch, V.J.S., Keller, G.R., and Brister, B.S., 2004, Gravity and aeromagnetic expression of tectonic and volcanic elements of the southern San Luis Basin, New Mexico and Colorado, *in* Brister, B., Bauer, P., Read, A., and Lueth, V., eds., Geology of the Taos Region: New Mexico Geological Society 55th Fall Field Conference Guidebook: Socorro, New Mexico, New Mexico Geological Society, p. 230–243.

Grauch, V.J.S., Bauer, P.W., Drenth, B.J., and Kelson, K.I., 2017, A shifting rift—Geophysical insights into the evolution of Rio Grande rift margins and the Embudo transfer zone near Taos, New Mexico: Geosphere, v. 13, no. 3, p. 870–910, https://doi.org/10.1130/GES01425.1.

Hallett, R.B., 1994, Volcanic Geology, Paleomagnetism, Geochronology and Geochemistry of the Rio Puerco Necks, West-Central New Mexico [Ph.D. dissertation]: Socorro, New Mexico, New Mexico Institute of Mining and Technology, 340 p.

Hallett, R.B., Kyle, P.R., and McIntosh, W.C., 1997, Paleomagnetic and $^{40}Ar/^{39}Ar$ age constraints on the chronologic evolution of the Rio Puerco volcanic necks and Mesa Prieta, west-central New Mexico: Implications for transition zone magmatism: Geological Society of America Bulletin, v. 109, p. 95–106, https://doi.org/10.1130/0016-7606(1997)109<0095:PAAAAC>2.3.CO;2.

Hansen, S.M., Dueker, K.G., Stachnik, J.C., Aster, R.C., and Karlstrom, K.E., 2013, A rootless Rockies—Support and lithospheric structure of the Colorado Rocky Mountains inferred from CREST and TA seismic data: Geochemistry Geophysics Geosystems, v. 14, no. 8, p. 2670–2695, https://doi.org/10.1002/ggge.20143.

Harrison, R.W., and Cikoski, C.T., 2012, Preliminary Geologic Map of the Winston Quadrangle, Sierra County, New Mexico: New Mexico Bureau of Geology and Mineral Resources Open-File Geologic Map 230, scale 1:24,000.

Haxby, W.F., and Turcotte, D.L., 1978, On isostatic geoid anomalies: Journal of Geophysical Research, v. 83, p. 5473–5478, https://doi.org/10.1029/JB083iB11p05473.

Henry, C.D., and Price, J.G., 1986, Early Basin and Range development in Trans-Pecos Texas and adjacent Chihuahua: Magmatism and orientation, timing, and style of extension: Journal of Geophysical Research, v. 91, p. 6213–6224, https://doi.org/10.1029/JB091iB06p06213.

House, M.A., Kelley, S.A., and Roy, M., 2003, Refining the footwall cooling history of a rift flank uplift, Rio Grande rift, New Mexico: Tectonics, v. 22, no. 5, p. 14-1–14-18, https://doi.org/10.1029/2002TC001418.

Ingersoll, R.V., 2001, Structural and stratigraphic evolution of the Rio Grande rift, northern New Mexico and southern Colorado: International Geology Review, v. 43, p. 867–891, https://doi.org/10.1080/00206810109465053.

Izett, G.A., and Obradovich, J.D., 1994, $^{40}Ar/^{39}Ar$ age constraints for the Jaramillo Normal subchron and Matuyama-Brunhes geomagnetic boundary: Journal of Geophysical Research, v. 99, p. 2925–2934, https://doi.org/10.1029/93JB03085.

Jochems, A.P., 2015, Geologic Map of the Williamsburg NW 7.5-Minute Quadrangle, Sierra County, New Mexico: New Mexico Bureau of Geology and Mineral Resources Open-File Geologic Map 251, scale 1:24,000.

Jochems, A.P., 2017, Geologic Map of the Arroyo Cuervo 7.5-Minute Quadrangle, Sierra County, New Mexico: New Mexico Bureau of Geology and Mineral Resources Open-File Geologic Map 261, scale 1:24,000.

Jochems, A.P., and Koning, D.J., 2015, Geologic Map of the Williamsburg 7.5-Minute Quadrangle, Sierra County, New Mexico: New Mexico Bureau of Geology and Mineral Resources Open-File Geologic Map 250, scale 1:24,000.

Jochems, A.P., and Koning, D.J., 2016, Geologic Map of the Saladone Tank 7.5-Minute Quadrangle, Sierra County, New Mexico: New Mexico Bureau of Geology and Mineral Resources Open-File Geologic Map 259, scale 1:24,000.

Jochems, A.P., and Koning, D.J., 2017, Geologic Map of the Clark Spring 7.5-Minute Quadrangle, Sierra County, New Mexico: New Mexico Bureau of Geology and Mineral Resources Open-File Geologic Map 263, scale 1:24,000.

Karlstrom, K.E., Coblentz, D., Dueker, K., Ouimet, W., Kirby, E., Van Wijk, J., Schmandt, B., Kelley, S., Lazear, G., Crossey, L.J., and Crow, R., 2012, Surface response to mantle convection beneath the Colorado Rocky Mountains and Colorado Plateau: Lithosphere, v. 4, p. 3–22, https://doi.org/10.1130/L150.1.

Kelley, S.A., and Chapin, C.E., 1995, Apatite fission-track thermochronology of the southern Rocky Mountain–Rio Grande rift–western High Plains province, *in* Bauer, P.W., Kues, B.S, Dunbar, N.W., Karlstrom, K.E., and Harrison, B., eds., Geology of the Santa Fe Region: New Mexico Geological Society 46th Annual Field Conference Guidebook: Socorro, New Mexico, New Mexico Geological Society, p. 87–96.

Kelley, S.A., Chapin, C.E., and Corrigan, J., 1992, Late Mesozoic to Cenozoic Cooling Histories of the Flanks of the Northern and Central Rio Grande Rift, Colorado and New Mexico: New Mexico Bureau of Mines and Mineral Resources Bulletin 145, 39 p.

Kelley, V.C., 1952, Tectonics of the Rio Grande depression of central New Mexico, *in* Johnson, R.B., and Read, C., eds., Rio Grande Country: New Mexico Geological Society Guidebook 3: Socorro, New Mexico, New Mexico Geological Society, p. 92–105.

Kelson, K.I., Hemphill-Haley, M.A., Olig, S.S., Simpson, G.D., Gardner, J.N., Reneau, S.L., Kolbe, T.R., Forman, S.L., and Wong, I.G., 1996, Late-Pleistocene and possibly Holocene displacement along the Rendija Canyon fault, Los Alamos County, New Mexico, *in* Goff, F., Kues, B.S., Rogers, M.A., McFadden, L.D., and Gardner, J.N., eds., The Jemez Mountains Region: New Mexico Geological Society 47th Field Conference Guidebook: Socorro, New Mexico, New Mexico Geological Society, p. 153–160.

Kelson, K.I., Hitchcock, C.S., and Harrison, J.B.J., 1999, Paleoseismology of the Tijeras fault near Golden, New Mexico, *in* Pazzaglia, F.J., and Lucas, S.G., eds., Albuquerque Geology: New Mexico Geological Society 50th Field Conference Guidebook: Socorro, New Mexico, New Mexico Geological Society, p. 201–210.

Kelson, K.I., Bauer, P.W., Unruh, J.R., and Bott, J.D.J., 2004, Late Quaternary characteristics of the northern Embudo fault, Taos County, New Mexico, *in* Brister, B., Bauer, P., Read, A., and Lueth, V., eds., Geology of the Taos Region: New Mexico Geological Society 55th Field Conference Guidebook: Socorro, New Mexico, New Mexico Geological Society, p. 147–157.

Kluth, C.F., and Schaftenaar, C.H., 1994, Depth and geometry of the northern Rio Grande rift in the San Luis Basin, south-central Colorado, *in* Keller, G.R., and Cather, S.M., eds., Basins of the Rio Grande Rift: Structure, Stratigraphy, and Tectonic Setting: Geological Society of America Special Paper 291, p. 27–38, https://doi.org/10.1130/SPE291-p27.

Koning, D.J., 1999, Fault segmentation and paleoseismicity of the southern Alamogordo fault, southern Rio Grande rift, New Mexico [M.S. thesis]: University of New Mexico Albuquerque, 286 p.

Koning, D.J., 2004, Geologic Map of the Lyden 7.5-Minute Quadrangle, Rio Arriba and Santa Fe Counties, New Mexico: New Mexico Bureau of Geology and Mineral Resources Open-File Geologic Map OF-GM-83, scale 1:24,000.

Koning, D.J., 2009, Geologic Map of the Three Rivers 7.5-Minute Quadrangle, Otero County, New Mexico: New Mexico Bureau of Geology and Mineral Resources Open-File Geologic Map OF-GM-187, scale 1:24,000.

Koning, D.J., 2012, The Santa Fe Group in the northern Winston graben, southwest New Mexico, and how changing Rio Grande rift tectonism may have influenced its deposition and erosion, *in* Lucas, S., McLemore, V., Lueth, V., Spielmann, J., and Krainer, K., eds., Warm Springs Region: New Mexico Geological Society 63rd Field Conference Guidebook: Socorro, New Mexico, New Mexico Geological Society, p. 457–474.

Koning, D.J., and Aby, S., 2003 (revised June 2004), Geologic Map of the Velarde 7.5-Minute Quadrangle, Rio Arriba and Taos Counties, New Mexico: New Mexico Bureau of Geology and Mineral Resources Open-File Geologic Map OF-GM-79, scale 1:24,000.

Koning, D.J., and Manley, K., 2003 (revised December 2005), Geologic Map of the San Juan Pueblo 7.5-Minute Quadrangle, Rio Arriba and Santa Fe Counties, New Mexico: New Mexico Bureau of Geology and Mineral Resources Open-File Geologic Map OF-GM-70, scale 1:24,000.

Koning, D.J., and Pazzaglia, F.J., 2002, Paleoseismicity of the Alamogordo fault along the Sacramento Mountains, southern Rio Grande rift, New Mexico, *in* Lueth, V., Giles, K., Lucas, S., Kues, B., Myers, R., and Ulmer-Scholle, D., eds., Geology of the White Sands: New Mexico Geological Society 53rd Field Conference Guidebook: Socorro, New Mexico, New Mexico Geological Society, p. 107–119.

Koning, D.J., and Read, A.S., 2010, Geologic Map of the Southern Española Basin: New Mexico Bureau of Geology and Mineral Resources Open-File Report 531, scale 1:48,000.

Koning, D.J., Connell, S.D., Pazzaglia, F.J., and McIntosh, W.C., 2002, Redefinition of the Ancha Formation and Pliocene-Pleistocene deposition in the Santa Fe embayment, north-central New Mexico: New Mexico Geology, v. 24, no. 3, p. 75–87.

Koning, D.J., Aby, S., and Kelson, K., 2007a, Preliminary Geologic Map of the Taos Junction Quadrangle, Taos County, New Mexico: New Mexico Bureau of Geology and Mineral Resources Open-File Geologic Map OF-GM-144, scale 1:24,000.

Koning, D.J., Karlstrom, K.E., Salem, A., and Lombardi, C., 2007b, Preliminary Geologic Map of the La Madera Quadrangle, Rio Arriba County, New Mexico: New Mexico Bureau of Geology and Mineral Resources Open-File Geologic Map OF-GM-141, scale 1:12,000.

Koning, D.J., McIntosh, W., and Dunbar, N., 2011, Geology of southern Black Mesa, Española Basin, New Mexico: New stratigraphic age control and interpretations of the southern Embudo fault system of the Rio Grande rift, *in* Koning, G., Karlstrom, K., Kelley, S., Lueth, V., and Aby, S., eds., Geology of the Tusas Mountains and Ojo Caliente: New Mexico Geological Society 62nd Field Conference Guidebook: Socorro, New Mexico, New Mexico Geological Society, p. 191–214.

Koning, D.J., Grauch, V.J.S., Connell, S.D., Ferguson, J., McIntosh, W., Slate, J.L., Wan, E., and Baldridge, W.S., 2013, Structure and tectonic evolution of the eastern Española Basin, Rio Grande rift, north-central New Mexico, *in* Hudson, M., and Grauch, V.J.S., eds., New Perspectives on the Rio Grande Rift: From Tectonics to Groundwater: Geological Society of America Special Paper 494, p. 185–219, https://doi.org/10.1130/2013.2494(08).

Koning, D.J., Rawling, G.C., Kelley, S., Goff, F., McIntosh, W., and Peters, L., 2014, Structure and tectonic evolution of the Sierra Blanca basin, *in* Rawling, G., McLemore, V., Timmons, S., and Dunbar, N., eds., Geology of the Sacramento Mountains Region: New Mexico Geological Society 65th Field Conference Guidebook: Socorro, New Mexico, New Mexico Geological Society, p. 209–226.

Koning, D.J., Jochems, A.P., and Cikoski, C., 2015, Geologic Map of the Skute Stone Arroyo 7.5-Minute Quadrangle, Sierra County, New Mexico: New Mexico Bureau of Geology and Mineral Resources Open-File Geologic Map 252, scale 1:24,000.

Koning, D.J., Aby, S., Grauch, V.J.S., and Zimmerer, M.J., 2016a, Latest Miocene–earliest Pliocene evolution of the ancestral Rio Grande at the Española–San Luis Basin boundary, northern New Mexico: New Mexico Geology, v. 38, no. 2, p. 24–49.

Koning, D.J., Jochems, A.P., Morgan, G.S., Lueth, V., and Peters, L., 2016b, Stratigraphy, gravel provenance, and age of early Rio Grande deposits exposed 1–2 km northwest of downtown Truth or Consequences, New Mexico, *in* Frey, B.A., Karlstrom, K.E., Lucas, S.G., Williams, S., Ziegler, K., McLemore, V., and Ulmer-Scholle, D., eds., The Geology of the Belen Area: New Mexico Geological Society 67th Annual Field Conference Guidebook: Socorro, New Mexico, New Mexico Geological Society, p. 459–478.

Koptev, A., Calais, E., Burov, E., Leroy, S., and Gerya, T., 2015, Dual continental rift systems generated by plume-lithosphere interaction: Nature Geoscience, v. 8, p. 388–392, https://doi.org/10.1038/ngeo2401.

Lavier, L., and Buck, R., 2002, Half graben versus large-offset low-angle normal fault: Importance of keeping cool during normal faulting: Journal of Geophysical Research, v. 107, p. ETG 8-1–ETG 8-13, https://doi.org/10.1029/2001JB000513.

Leonard, E.M., Hubbard, M.S., Kelley, S.A., Evanoff, E., Siddoway, C.S., Oviatt, C.G., Heizler, M., and Timmons, M., 2002, High Plains to Rio Grande rift: Late Cenozoic evolution of central Colorado, *in* Lageson, D., ed., Science at the Highest Level: Geological Society of America Field Guide 3, p. 59–93, https://doi.org/10.1130/0-8137-0003-5.59.

Lipman, P.W., and Mehnert, H.H., 1975, Late Cenozoic basaltic volcanism and development of the Rio Grande depression in the southern Rocky Mountains, *in* Curtis, B.F., ed., Cenozoic History of the Southern Rocky Mountains: Geological Society of America Memoir 144, p. 119–154, https://doi.org/10.1130/MEM144-p119.

Liu, S., and Currie, C., 2016, Farallon plate dynamics prior to the Laramide orogeny: Numerical models of flat subduction: Tectonophysics, v. 666, p. 33–47, https://doi.org/10.1016/j.tecto.2015.10.010.

Love, D.W., Allen, B.D., Lucas, S.G., Morgan, G.S., and Myers, R.G., 2012, New perspectives on the geology and paleontology of ice-age Lake Otero, Tularosa Basin, south-central New Mexico, *in* Greenwald, D., 2010 Tularosa Basin Conference Proceedings: The Land of Enchantment through Time and Space: Tularosa, New Mexico, Jornada Research Institute, 13 p.

Lozinsky, R.P., and Tedford, R.H., 1991, Geology and Paleontology of the Santa Fe Group, Southwestern Albuquerque Basin, Valencia County, New Mexico: New Mexico Bureau of Mines and Mineral Resources Bulletin 132, 35 p.

Lucas, S.G., and Ingersoll, R.V., 1981, Cenozoic continental deposits of New Mexico: An overview: Geological Society of America Bulletin, v. 92, p. 917–932, https://doi.org/10.1130/0016-7606(1981)92<917:CCDONM>2.0.CO;2.

Lueth, V.W., Chamberlin, R., Peters, L., and Love, D.W., 2016, An $^{40}Ar/^{39}Ar$ age and paleogeographic setting for the Riley travertine, Socorro County, New Mexico, *in* Frey, B.A., Karlstrom, K.E., Lucas, S.G., William, S., Ziegler, K., McLemore, V., and Ulmer-Scholle, D.S., eds., The Geology of the Belen Area: New Mexico Geological Society 67th Annual Field Conference Guidebook: Socorro, New Mexico, New Mexico Geological Society, p. 58–61.

MacCarthy, J.K., Aster, R.C., Dueker, K., Hansen, S., Schmandt, B., and Karlstrom, K., 2014, Seismic tomography of the Colorado Rocky Mountains upper mantle from CREST: Lithosphere–asthenosphere interactions and mantle support of topography: Earth and Planetary Science Letters, v. 402, p. 107–119, https://doi.org/10.1016/j.epsl.2014.03.063.

MacFadden, B.J., 1992, Fossil Horses: Systematics, Paleobiology, and Evolution of the Family Equidae: New York, Cambridge University Press, 369 p.

Machette, M.N., 1978, Geological Map of the San Acacia Quadrangle, Socorro County, New Mexico: U.S. Geological Survey Quadrangle Map GQ-1415, scale 1:24,000.

Machette, M.N., 1986, History of Quaternary offset and paleoseismicity along the La Jencia fault, central Rio Grande rift, New Mexico: Bulletin of the Seismological Society of America, v. 76, p. 259–272.

Machette, M.N., 1987, Preliminary Assessment of Quaternary Faulting near Truth or Consequences, New Mexico: U.S. Geological Survey Open-File Report 87–652, 40 p.

Machette, M.N., Personius, S.F., Kelson, K.I., Dart, R.L., and Haller, K.M., 1998, Map and Data for Quaternary Faults and Folds in New Mexico: U.S. Geological Survey Open-File Report 98–521, 451 p.

Mack, G.H., Nightingale, A.L., Seager, W.R., and Clemons, R.E., 1994a, The Oligocene Goodsight–Cedar Hills half graben near Las Cruces and its implications to the evolution of the Mogollon-Datil volcanic field and to the southern Rio Grande rift: New Mexico Geological Society 45th Field Conference Guidebook: Socorro, New Mexico, New Mexico Geological Society, p. 135–142.

Mack, G.H., Seager, W.R., and Kieling, J., 1994b, Late Oligocene and Miocene faulting and sedimentation, and evolution of the southern Rio Grande rift, New Mexico, USA: Sedimentary Geology, v. 92, p. 79–96, https://doi.org/10.1016/0037-0738(94)90055-8.

Mack, G.H., Salyards, S.L., McIntosh, W.C., and Leeder, M.R., 1998, Reversal magnetostratigraphy and radioisotopic geochronology of the Plio-Pleistocene Camp Rice and Palomas Formations, southern Rio Grande rift, *in* Mack, G., Austin, G., and Barker, J., eds., Las Cruces County II: New Mexico Geological Society 49th Field Conference Guidebook: Socorro, New Mexico, New Mexico Geological Society, p. 229–236.

Mack, G.H., Seager, W.R., Leeder, M.R., Perez-Arclucea, M., and Salyards, S.L., 2006, Pliocene and Quaternary history of the Rio Grande, the axial river of the southern Rio Grande rift, New Mexico, USA: Earth-Science Reviews, v. 79, p. 141–162, https://doi.org/10.1016/j.earscirev.2006.07.002.

Maldonado, F., Slate, J.L., Love, D.W., Connell, S.D., Cole, J.C., and Karlstrom, K.E., 2007, Geologic Map of the Pueblo of Isleta Tribal Lands and Vicinity, Bernalillo, Torrance, and Valencia Counties, central New Mexico: U.S. Geological Survey Scientific Investigations Map 2913, scale 1:50,000.

Maldonado, F., Miggins, D.P., and Budahn, J.R., 2013, Deformational and erosional history for the Abiquiu and contiguous area, north-central New Mexico: Implications for formation of the Abiquiu embayment and a discussion of new geochronological and geochemical analyses, *in* Hudson, M., and Grauch, V.J.S., eds., New Perspectives on the Rio Grande Rift: From Tectonics to Groundwater: Geological Society of America Special Paper 494, p. 125–155, https://doi.org/10.1130/2013.2494(06).

Manley, K., 1979, Tertiary and Quaternary stratigraphy of the Northeast Plateau, Española Basin, New Mexico, *in* Ingersoll, R.V., Woodward, LA., and James, H.L., eds., Guidebook of Santa Fe Country: New Mexico Geological Society 30th Annual Field Conference Guidebook: Socorro, New Mexico, New Mexico Geological Society, p. 231–236.

McCalpin, J., 1982, Quaternary Geology and Neotectonics of the West Flank of the Northern Sangre de Cristo Mountains, South-Central Colorado: Colorado School of Mines Quarterly, v. 77, 89 p.

McCalpin, J., 1986, Quaternary tectonics of the Sangre de Cristo and Villa Grove Fault Zones, *in* Rogers, W.P., and Kirkham, R.M., eds., Contributions to Colorado Seismicity and Tectonics—A 1986 update: Colorado Geological Survey Special Publication, v. 28, p. 59–64.

McCalpin, J.P., ed., 1996, Paleoseismology: New York, Academic Press, 583 p.

McCalpin, J.P., 1997, Paleoseismicity of Quaternary Faults near Albuquerque, New Mexico: Final technical report submitted to U.S. Geological Survey by GEO-HAZ Consulting, Inc., Contract 1434-HQ-96-GR-02751, October 6, 1997, 18 p.

McCalpin, J.P., 2005, Late Quaternary activity of the Pajarito fault, Rio Grande rift of northern New Mexico, USA: Tectonophysics, v. 408, p. 213–236, https://doi.org/10.1016/j.tecto.2005.05.038.

McCalpin, J.P., 2006, Quaternary Faulting and Seismic Source Characterization in the El Paso–Juarez Metropolitan Area; Collaborative Research with the University of Texas at El Paso, Program Element II: Evaluate Urban Hazard and Risk: Final Technical Report, National Earthquake Hazards Reduction Program, U.S. Geological Survey, 68 p.

McCalpin, J.P., and Harrison, J.B.J., 2001, Paleoseismicity of Quaternary Faults near Albuquerque, New Mexico: Final technical report submitted to U.S. Geological Survey by GEO-HAZ Consulting, Contract 99-HQ-GR-0056, August 4, 2001, 58 p.

McCalpin, J.P., and Harrison, J.B.J., 2006, Paleoseismicity of the Sandia Fault Zone, Albuquerque, New Mexico: Crestone, Colorado, GEO-HAZ Consulting, 38 p.

McCalpin, J.P., Harrison, J.B.J., Berger, G.W., and Tobin, H.C., 2011, Paleoseismicity of a low-slip-rate normal fault in the Rio Grande rift, USA: The Calabacillas fault, Albuquerque, New Mexico, *in* Audemard, M., Michetti, F.A., and McCalpin, J.P., eds., Geologic Criteria for Evaluating Seismicity Revisited: Forty Years of Paleoseismic Investigations and the Natural Record of Past Earthquakes: Geological Society of America Special Paper 479, p. 23–46, https://doi.org/10.1130/2011.2479(01).

McCraw, D.J., and Love, D.W., 2012, An overview and delineation of the Cuchillo geomorphic surface, Engle and Palomas Basins, New Mexico, *in* Lucas, S.G., McLemore, V.T., Lueth, V.W., Spielmann, J.A., and Krainer, K., eds., Warm Springs Region: New Mexico Geological Society 63rd Field Conference Guidebook: Socorro, New Mexico, New Mexico Geological Society, p. 491–498.

McKenzie, D.P., Watts, A., Parsons, B., and Roufosse, M., 1980, Planform of mantle convection beneath the Pacific Ocean: Nature, v. 288, p. 442–446, https://doi.org/10.1038/288442a0.

McLemore, V.T., Heizler, M., Love, D.W., Cikoski, C.T., and Koning, D.J., 2012, $^{40}Ar/^{39}Ar$ ages of selected basalts in the Sierra Cuchillo and Mud Springs Mountains, Sierra and Socorro Counties, New Mexico, *in* Lucas, S.G., McLemore, V.T., Lueth, V.W., Spielmann, J.A., and Krainer, K., eds., Warm Springs Region: New Mexico Geological Society 63rd Field Conference Guidebook: Socorro, New Mexico, New Mexico Geological Society, p. 285–292.

McMillan, M.E., Angevine, C.L., and Heller, P.L., 2002, Postdepositional tilt of the Miocene–Pliocene Ogallala Group on the western Great Plains: Evidence of late Cenozoic uplift of the Rocky Mountains: Geology, v. 30, p. 63–66, https://doi.org/10.1130/0091-7613(2002)030<0063:PTOTMP>2.0.CO;2.

McMillan, M.E., Heller, P.L., and Wing, S.L., 2006, History and causes of post-Laramide relief in the Rocky Mountain orogenic plateau: Geological Society of America Bulletin, v. 118, p. 393–405, https://doi.org/10.1130/B25712.1.

McWhorter, D.B., and Sunada, D.K., 1977, Ground-Water Hydrology and Hydraulics: Fort Collins, Colorado, Water Resources Publication, 290 p.

Morgan, P., Seager, W.R., and Golombek, M.P., 1986, Cenozoic thermal, mechanical and tectonic evolution of the Rio Grande rift: Journal of Geophysical Research, v. 91, p. 6263–6276, https://doi.org/10.1029/JB091iB06p06263.

Moucha, R., Forte, A.M., Rowley, D.B., Mitrovica, J.X., Simmons, N.A., and Grand, S.P., 2008, Mantle convection and the recent evolution of the Colorado Plateau and the Rio Grande rift valley: Geology, v. 36, p. 439–442, https://doi.org/10.1130/G24577A.1.

Murray, K., Murray, M., Sheehan, A., Axen, G., and van Wijk, J., 2015, GPS measurements of deformation near the Rio Grande rift: Evidence for variations in the rate of extension: San

Francisco, California, American Geophysical Union, Fall Meeting supplement, abstract G13A-1015.
Nereson, A., Stroud, J., Karlstrom, K., Heizler, M., and McIntosh, W., 2013, Dynamic topography of the western Great Plains: Geomorphic and $^{40}Ar/^{39}Ar$ evidence for mantle-driven uplift associated with the Jemez Lineament of NE New Mexico and SE Colorado: Geosphere, v. 9, no. 3, p. 521–545, https://doi.org/10.1130/GES00837.1.
New Mexico Bureau of Geology and Mineral Resources, 2003, Geologic Map of New Mexico: Socorro, New Mexico, New Mexico Bureau of Geology and Mineral Resources, published in cooperation with the U.S. Geological Survey, scale 1:500,000.
Ockendon, J.R., and Turcotte, D.L., 1977, On the gravitational potential and field anomalies due to thin mass layers: Geophysical Journal International, v. 48, p. 479–492, https://doi.org/10.1111/j.1365-246X.1977.tb03684.x.
Olig, S.S., Eppes, M.C., Forman, S.L., Love, D.W., and Allen, B.D., 2011, Late Quaternary earthquakes on the Hubbell Spring fault system, New Mexico, USA: Evidence for noncharacteristic ruptures of intrabasinal faults in the Rio Grande rift, *in* Audemard, M., Michetti, F.A., and McCalpin, J.P., eds., Geologic Criteria for Evaluating Seismicity Revisited: Forty Years of Paleoseismic Investigations and the Natural Record of Past Earthquakes: Geological Society of America Special Paper 479, p. 47–77, https://doi.org/10.1130/2011.2479(02).
Olmsted, B.W., and McIntosh, W.C., 2004, $^{40}Ar/^{39}Ar$ Geochronology of the Ocate Volcanic Field, North-Central New Mexico: New Mexico Bureau of Geology and Mineral Resources Bulletin 160, p. 297–308.
O'Neill, J.M., 1998, Late Cenozoic Physiographic Evolution of the Ocate Volcanic Field: U.S. Geological Survey Professional Paper 1478-B, p. B1–B15.
Oskin, M., and Stock, J., 2003, Marine incursion synchronous with plate-boundary localization in the Gulf of California: Geology, v. 31, p. 23–26, https://doi.org/10.1130/0091-7613(2003)031<0023:MISWPB>2.0.CO;2.
Personius, S.F., and Mahan, S.A., 2003, Paleoearthquakes and eolian-dominated fault sedimentation along the Hubbell Spring fault zone near Albuquerque, New Mexico: Bulletin of the Seismological Society of America, v. 93, p. 1355–1369, https://doi.org/10.1785/0120020031.
Personius, S.F., Machette, M.N., and Kelson, K.I., 1999, Quaternary faults in the Albuquerque area—An update, *in* Pazzaglia, F., and Lucas, S., eds., Albuquerque Geology: New Mexico Geological Society 50 Field Conference Guidebook: Socorro, New Mexico, New Mexico Geological Society, p. 189–200.
Phillips, F.M., Ayarbe, J.P., Harrison, J.B.J., and Elmore, D., 2003, Dating rupture events on alluvial fault scarps using cosmogenic nuclides and scarp morphology: Earth and Planetary Science Letters, v. 215, p. 203–218, https://doi.org/10.1016/S0012-821X(03)00419-9.
Reneau, S.L., Gardner, J.N., Lavine, A., McDonald, E.V., Lewis, C., Katzman, D., WoldeGabriel, G., Krier, D., Bergfeld, D., and Heikoop, J., 2002, Paleoseismic Investigation of Trench EOC-2, Pajarito Fault Zone, Los Alamos National Laboratory, New Mexico: Los Alamos National Laboratory Report LA-13939-MS, 65 p.
Repasch, M., Karlstrom, K., Heizler, M., and Pecha, M., 2017, Birth and evolution of the Rio Grande fluvial system in the past 8 Ma: Progressive downward integration and the influence of tectonics, volcanism, and climate: Earth-Science Reviews, v. 168, p. 113–164, https://doi.org/10.1016/j.earscirev.2017.03.003.
Ricketts, J.W., and Karlstrom, K., 2016, Processes controlling the development of the Rio Grande rift at long timescales, *in* Frey, B.A., Karlstrom, K.E., Lucas, S.G., William, S., Ziegler, K., McLemore, V., and Ulmer-Scholle, D.S., eds., Geology of the Belen Area: New Mexico Geological Society 67th Field Conference Guidebook: Socorro, New Mexico, New Mexico Geological Society, p. 195–202.
Ricketts, J.W., Karlstrom, K.E., Priewisch, A., Crossey, L.J., Polyak, V.J., and Asmerom, Y., 2014, Quaternary extension in the Rio Grande rift at elevated strain rates recorded in travertine deposits, central New Mexico: Lithosphere, v. 6, p. 3–16, https://doi.org/10.1130/L278.1.
Ricketts, J.W., Kelley, S.A., Karlstrom, K.E., Schmandt, B., Donahue, M.S., and van Wijk, J., 2015, Synchronous opening of the Rio Grande rift along its entire length at 25–10 Ma supported by apatite (U-Th)/He and fission-track thermochronology, and evaluation of possible driving mechanisms: Geological Society of America Bulletin, v. 128, p. 397–424, https://doi.org/10.1130/B31223.1.
Rowan, E.L., Hayba, D.O., Nelson, P.H., Burns, W.M., and Houseknecht, D.W., 2003, Sandstone and Shale Compaction Curves Derived from Sonic and Gamma Ray Logs in Offshore Wells, North Slope, Alaska—Parameters for Basin Modeling: U.S. Geological Survey Open-File Report 03–329, available at http://pubs.usgs.gov/of/2003/of03-329/.
Roy, M., Kelley, S., Pazzaglia, F., Cather, S., and House, M., 2004, Middle Tertiary buoyancy modification and its relationship to rock exhumation, cooling, and subsequent extension at the eastern margin of the Colorado Plateau: Geology, v. 32, p. 925–928, https://doi.org/10.1130/G20561.1.
Ruleman, C., and Machette, M.N., 2007, An overview of the Sangre de Cristo fault system and new insights to interactions between Quaternary faults in the northern Rio Grande rift, *in* Machette, M.N., Coates, M.M., and Johnson, M.L., eds., 2007 Rocky Mountain Section Friends of the Pleistocene Field Trip—Quaternary Geology of the San Luis Basin of Colorado and New Mexico, September 7–9: U.S. Geological Survey Open-File Report 2007-1193, p. 187–197.
Ruleman, C.A., Thompson, R.A., Shroba, R.R., Anderson, M., Drenth, B.J., Rotzien, J., and Lyon, J., 2013, Late Miocene–Pleistocene evolution of a Rio Grande rift subbasin, Sunshine Valley–Costilla Plain, San Luis Basin, New Mexico and Colorado, *in* Hudson, M.R., and Grauch, V.J.S., eds., New Perspectives on Rio Grande Rift Basins: From Tectonics to Groundwater: Geological Society of America Special Paper 494, p. 47–73, https://doi.org/10.1130/2013.2494(03).
Russell, L.R., and Snelson, S., 1994, Structure and tectonics of the Albuquerque Basin segment of the Rio Grande rift: Insights from reflection seismic data, *in* Keller, G.R., and Cather, S.M., eds., Basins of the Rio Grande Rift: Structure, Stratigraphy, and Tectonic Setting: Geological Society of America Special Paper 291, p. 83–112, https://doi.org/10.1130/SPE291-p83.
Sandwell, D.T., and MacKenzie, K.R., 1989, Geoid height versus topography for oceanic plateaus and swells: Journal of Geophysical Research, v. 94, p. 7403–7418, https://doi.org/10.1029/JB094iB06p07403.
Sandwell, D.T., and Renkin, M.L., 1988, Compensation of swells and plateaus in the North Pacific: No direct evidence for mantle convection: Journal of Geophysical Research, v. 93, p. 2775–2783, https://doi.org/10.1029/JB093iB04p02775.
Sanford, A.R., Lin, K.W., Tsai, I.C., and Jaksha, L.H., 2002, Earthquake catalogs for New Mexico and bordering areas: 1869–1998: Socorro, New Mexico, New Mexico Bureau of Geology and Mineral Resources, New Mexico Institute of Mining and Technology, p. 1–9.
Seager, W.R., and Hawley, J.W., 1973, Geology of Rincon Quadrangle, New Mexico: New Mexico Bureau of Mines and Mineral Resources Bulletin 101, 42 p., map scale 1:24,000.
Seager, W.R., and Mack, G.H., 1991, Geology of Garfield Quadrangle, Sierra and Doña Ana Counties, New Mexico: New Mexico Bureau of Mines and Mineral Resources Bulletin 128, 24 p., map scale 1:24,000.
Seager, W.R., and Mack, G.H., 2003, Geology of the Caballo Mountains, New Mexico: New Mexico Bureau of Geology and Mineral Resources Memoir 49, 136 p.
Seager, W.R., Hawley, J.W., and Clemons, R.E., 1971, Geology of San Diego Mountain Area, Doña Ana County, New Mexico: New Mexico Bureau of Mines and Mineral Resources Bulletin 97, 38 p. and 2 plates.
Seager, W.R., Clemons, R.E., and Hawley, J.W., 1975, Geology of Sierra Alta Quadrangle, Dona Ana County, New Mexico: New Mexico Bureau of Mines and Mineral Resources Bulletin 102, 56 p. and 1:24,000 scale map.
Seager, W.R., Shafiqullah, M., Hawley, J.W., and Marvin, R.F., 1984, New K-Ar dates from basalts and the evolution of the southern Rio Grande rift: Geological Society of America Bulletin, v. 95, p. 87–99, https://doi.org/10.1130/0016-7606(1984)95<87:NKDFBA>2.0.CO;2.
Sleep, N.H., 2011, Seismically observable features of mature stagnant-lid convection at the base of the lithosphere: Some scaling relationships: Geochemistry Geophysics Geosystems, v. 12, Q10018, https://doi.org/10.1029/2011GC003760.
Smith, G.A., 2004, Middle to late Cenozoic development of the Rio Grande rift and adjacent regions in northern New Mexico, *in* Mack, G.H., and Giles, K.A., eds., The Geology of New Mexico: A Geologic History: New Mexico Geological Society Special Publication 11, p. 331–358.
Smith, G.A., and Kuhle, A.J., 1998 (29 February 2000 revision), Geology of Santo Domingo Pueblo and Santo Domingo Pueblo SW Quadrangle, Sandoval County, New Mexico: New Mexico Bureau of Geology and Mineral Resources Open-File Geologic Maps OF-GM-15 and OF-GM-26, scale 1:24,000.
Smith, G.A., and Roy, M., 2001, Assessing ruptured hanging-wall hinge-zone uplifts in the northern Rio Grande rift, New Mexico [abs.]: Geological Society of America Abstracts with Programs, v. 33, no. 5, p. 61.
Smith, G.A., McIntosh, W., and Kuhle, A.J., 2001, Sedimentologic and geomorphic evidence for seesaw subsidence of the Santo Domingo accommodation-zone basin, Rio Grande rift, New

Mexico: Geological Society of America Bulletin, v. 113, no. 5, p. 561–574, https://doi.org/10.1130/0016-7606(2001)113<0561:SAGEFS>2.0.CO;2.
Smith, G.A., Moore, J.D., and McIntosh, W.C., 2002, Assessing roles of volcanism and basin subsidence in causing Oligocene–Lower Miocene sedimentation in the northern Rio Grande rift, New Mexico, U.S.A.: Journal of Sedimentary Research, v. 72, p. 836–848, https://doi.org/10.1306/050602720836.
Spell, T.L., Kyle, P.R., and Baker, J., 1996a, Geochronology and geochemistry of the Cerro Toledo Rhyolite, *in* Goff, F., Kues, B., Rogers, M., McFadden, L., Gardner, J., eds., Jemez Mountains Region: New Mexico Geological Society 47th Field Conference Guidebook: Socorro, New Mexico, New Mexico Geological Society, p. 263–268.
Spell, T., McDougall, I., and Doulgeris, A., 1996b, Cerro Toledo Rhyolite, Jemez volcanic field, New Mexico: Ar geochronology of eruptions between two caldera-forming events: Geological Society of America Bulletin, v. 108, p. 1549–1566, https://doi.org/10.1130/0016-7606(1996)108<1549:CTRJVF>2.3.CO;2.
Spiegel, Z., and Baldwin, B., 1963, Geology and Water Resources of the Santa Fe Area, New Mexico: U.S. Geological Survey Water-Supply Paper 1525, 258 p.
Stearns, C.E., 1953, Tertiary geology of the Galisteo-Tonque area, New Mexico: Geological Society of America Bulletin, v. 64, p. 459–508, https://doi.org/10.1130/0016-7606(1953)64[459:TGOTGA]2.0.CO;2.
Stearns, C.E., 1979, New K-Ar dates and the late Pliocene to Holocene geomorphic history of the central Rio Grande region, New Mexico: Geological Society of America Bulletin, v. 90, p. 799–800, https://doi.org/10.1130/0016-7606(1979)90<799:NKDATL>2.0.CO;2.
Steven, T.A., Evanoff, E., and Yuhas, R.H., 1997, Middle and late Cenozoic tectonic and geomorphic development of the Front Range of Colorado, *in* Bolyard, D.W., and Sonnenberg, S.A., eds., Geologic History of the Colorado Front Range: Denver, Colorado, Rocky Mountain Section, American Association of Petroleum Geologists, Field Trip 7, p. 115–124.
Stroud, J.R., 1997, Geochronology of the Raton-Clayton Volcanic Field, with Implications for Volcanic History and Landscape Evolution [M.S. thesis]: Socorro, New Mexico, New Mexico Institute of Mining and Technology, 164 p.
Thompson, R.A., Sawyer, D.A., Hudson, M.R., Grauch, V.J.S., and McIntosh, W.C., 2006, Cenozoic volcanism of the La Bajada constriction area, New Mexico, *in* Minor, S.A., ed., The Cerrillos Uplift, the La Bada Constriction, and Hydrogeologic Framework of the Santo Domingo Basin, Rio Grande Rift, New Mexico: U.S. Geological Survey Professional Paper 1720, p. 41–60.
Thompson, R.A., Shroba, R.R., Machette, M.N., Fridrich, C.J., Brandt, T.R., and Cosca, M.A., 2015, Geologic Map of the Alamosa 30′ × 60′ Quadrangle, South-Central Colorado: U.S. Geological Survey Scientific Investigations Map 3342, 23 p., scale 1:100,000.
Turcotte, D.L., and Emerman, S.H., 1983, Mechanisms of active and passive rifting: Tectonophysics, v. 94, no. 1–4, p. 39–50, https://doi.org/10.1016/0040-1951(83)90008-2.
Tweto, O., 1979, The Rio Grande rift system in Colorado, *in* Riecker, R.E., ed., Rio Grande Rift: Tectonics and Magmatism: American Geophysical Union Special Publication 14, p. 33–56, https://doi.org/10.1029/SP014p0033.
van Hinte, J.E., 1978, Geohistory analysis—Application of micropaleontology in exploration geology: American Association of Petroleum Geologists Bulletin, v. 62, p. 201–222.
van Wijk, J.W., 2005, Role of weak zone orientation in continental lithosphere extension: Geophysical Research Letters, v. 32, no. 2, https://doi.org/10.1029/2004GL022192.
van Wijk, J.W., Van Hunen, J., and Goes, S., 2008, Small-scale convection during continental rifting: Evidence from the Rio Grande rift: Geology, v. 36, p. 575–578, https://doi.org/10.1130/G24691A.1.
van Wijk, J.W., Baldridge, W.S., Van Hunen, J., Goes, S., Aster, R., Coblentz, D.D., Grand, S.P., and Ni, J., 2010, Small-scale convection at the edge of the Colorado Plateau: Implications for topography, magmatism, and evolution of Proterozoic lithosphere: Geology, v. 38, p. 611–614, https://doi.org/10.1130/G31031.1.
Webb, S.D., and Opdyke, N.D., 1995, Global climatic influences on Cenozoic land mammal faunas, *in* Stanley, S.M., et al., eds., Effects of Past Global Change on Life: Washington, D.C., National Academy Press, p. 184–208.
Wilson, D., Aster, R., West, M., Ni, J., Grand, S., Gao, W., Baldridge, W.S., Semken, S., and Patel, P., 2005, Lithospheric structure of the Rio Grande rift: Nature, v. 433, p. 851–855, https://doi.org/10.1038/nature03297.
WoldeGabriel, G., Warren, R.G., Broxton, D.E., Vaniman, D.T., Heizler, M.T., Kluk, E.C., and Peters, L., 2001, Episodic volcanism, petrology, and lithostratigraphy of the Pajarito Plateau and adjacent areas of the Española Basin and the Jemez Mountains, *in* Crumpler, L.S., and Lucas, S.G., eds., Volcanology in New Mexico: Museum of Natural History and Science Bulletin 18, p. 97–129.
WoldeGabriel, G., Warren, R.G., Cole, G., Goff, F., Broxton, D., Vaniman, D., Peters, L., Naranjo, A., and Kluk, E., 2006, Volcanism, Tectonics, and Chronostratigraphy in the Pajarito Plateau of the Española Basin, Rio Grande Rift, North Central New Mexico, US: Los Alamos National Laboratory Report LA-UR-06–6089, 122 p.
WoldeGabriel, G., Koning, D.J., Broxton, D., and Warren, R.G., 2013, Chronology of volcanism, tectonics, and sedimentation near the western boundary fault of the Española Basin, Rio Grande rift, New Mexico, *in* Hudson, M., and Grauch, V.J.S., eds., New Perspectives on the Rio Grande Rift: From Tectonics to Groundwater: Geological Society of America Special Paper 494, p. 221–238, https://doi.org/10.1130/2013.2494(09).
Wong, I., Kelson, K., Olig, S., Kolbe, T., Hemphill-Haley, M., Bott, J., Green, R., Kanakari, H., Sawyer, J., Silva, W., Stark, C., Haraden, C., Fenton, C., Unruh, J., Gardner, J., Reneau, S., and House, L., 1995, Seismic hazards evaluation of the Los Alamos National Laboratory; unpublished consulting report prepared for Los Alamos National Laboratory by Woodward-Clyde Federal Services, Oakland, California.
Wong, I., Olig, S., Dober, M., Silva, W., Wright, D., Thomas, P., Gregor, N., Sanford, A., Lin, K.W., and Love, D., 2004, Earthquake scenario and probabilistic ground-shaking hazard maps for the Albuquerque–Belen–Santa Fe, New Mexico, corridor: New Mexico Geology, v. 26, p. 3–33.
Wright, H.E., 1946, Tertiary and Quaternary geology of the lower Rio Puerco area, New Mexico: Geological Society of America Bulletin, v. 57, p. 383–456, https://doi.org/10.1130/0016-7606(1946)57[383:TAQGOT]2.0.CO;2.
Xie, X., and Heller, P., 2009, Plate tectonics and basin subsidence history: Geological Society of America Bulletin, v. 121, p. 55–64, https://doi.org/10.1130/B26398.1.